IMMUNODEFICIENCY

LTβR deficiency causes lymph node aplasia and impaired B cell differentiation

**Bernhard Ransmayr[1,2,3], Sevgi Köstel Bal[1,2,3], Marini Thian[1,2,3]†, Michael Svaton[1,2], Cheryl van de Wetering[1,2], Christoph Hafemeister[1], Anna Segarra-Roca[1], Jana Block[1,2,3], Alexandra Frohne[1], Ana Krolo[2,3]‡, Melek Yorgun Altunbas[4,5,6,7], Sevgi Bilgic-Eltan[4,5,6,7], Ayça Kıykım[8], Omer Aydiner[9], Selin Kesim[10], Sabahat Inanir[10], Elif Karakoc-Aydiner[4,5,6,7], Ahmet Ozen[4,5,6,7], Ümran Aba[11,12], Aylin Çomak[13], Gökçen Dilşa Tuğcu[14], Robert Pazdzior[2]§, Bettina Huber[15], Matthias Farlik[15], Stefan Kubicek[2], Horst von Bernuth[16,17,18,19], Ingrid Simonitsch-Klupp[20], Marta Rizzi[21,22,23], Florian Halbritter[1], Alexei V. Tumanov[24], Michael J. Kraakman[1,2,3], Ayşe Metin[25], Irinka Castanon[1,2], Baran Erman[11,12], Safa Baris[4,5,6,7], Kaan Boztug[1,2,3,26,27]*

Secondary lymphoid organs (SLOs) provide the confined microenvironment required for stromal cells to interact with immune cells to initiate adaptive immune responses resulting in B cell differentiation. Here, we studied three patients from two families with functional hyposplenism, absence of tonsils, and complete lymph node aplasia, leading to recurrent bacterial and viral infections. We identified biallelic loss-of-function mutations in *LTBR,* encoding the lymphotoxin beta receptor (LTβR), primarily expressed on stromal cells. Patients with LTβR deficiency had hypogammaglobulinemia, diminished memory B cells, regulatory and follicular T helper cells, and dysregulated expression of several tumor necrosis factor family members. B cell differentiation in an ex vivo coculture system was intact, implying that the observed B cell defects were not intrinsic in nature and instead resulted from LTβR-dependent stromal cell interaction signaling critical for SLO formation. Collectively, we define a human inborn error of immunity caused primarily by a stromal defect affecting the development and function of SLOs.

[1]St. Anna Children's Cancer Research Institute, Vienna, Austria. [2]CeMM Research Center for Molecular Medicine of the Austrian Academy of Sciences, Vienna, Austria. [3]Ludwig Boltzmann Institute for Rare and Undiagnosed Diseases, Vienna, Austria. [4]Department of Pediatrics, Division of Allergy and Immunology, Marmara University School of Medicine, Istanbul, Turkey. [5]Istanbul Jeffrey Modell Diagnostic Center for Primary Immunodeficiency Diseases, Istanbul, Turkey. [6]Işıl Berat Barlan Center for Translational Medicine, Marmara University, Istanbul, Turkey. [7]Marmara University, Immune Deficiency Application and Research Center, Istanbul, Turkey. [8]Istanbul University-Cerrahpasa, Faculty of Medicine, Department of Pediatric Allergy and Immunology, Istanbul, Turkey. [9]Kartal Dr. Lütfi Kırdar City Hospital, Department of Radiology, Istanbul, Turkey. [10]Marmara University, Faculty of Medicine, Department of Nuclear Medicine, Istanbul, Turkey. [11]Can Sucak Research Laboratory for Translational Immunology, Hacettepe University, Ankara, Turkey. [12]Institute of Child Health, Hacettepe University, Ankara, Turkey. [13]Ankara Bilkent City Hospital, Children's Hospital, Department of Nuclear Medicine, Ankara, Turkey. [14]Ankara Bilkent City Hospital, Children's Hospital, Department of Pediatric Pulmonology, Ankara, Turkey. [15]Medical University of Vienna, Department of Dermatology, Vienna, Austria. [16]Department of Pediatric Respiratory Medicine, Immunology and Critical Care Medicine, Charité University Medicine, Berlin, Corporate Member of Free University and Humboldt University and Berlin Institute of Health, Berlin, Germany. [17]Labor Berlin Charité-Vivantes, Department of Immunology, Berlin, Germany. [18]Berlin Institute of International Health Global Health Center Charité – Universitätsmedizin Berlin, Berlin, Germany. [19]Charité - Universitätsmedizin Berlin, corporate member of Freie Universität Berlin, Humboldt-Universität zu Berlin, and Berlin Institute of Health (BIH), Berlin-Brandenburg Center for Regenerative Therapies (BCRT), Berlin, Germany. [20]Medical University of Vienna, Department of Pathology, Vienna, Austria. [21]Department of Rheumatology and Clinical Immunology and Center for Chronic Immunodeficiency, Medical Center University of Freiburg, Faculty of Medicine, University of Freiburg, Freiburg, Germany. [22]CIBSS - Centre for Integrative Biological Signalling Studies, University of Freiburg, Freiburg, Germany. [23]Medical University of Vienna, Center for Pathophysiology, Infectiology and Immunology, Institute of Immunology, Vienna, Austria. [24]Department of Microbiology, Immunology, and Molecular Genetics, University of Texas Health Science Center at San Antonio, San Antonio, TX, USA. [25]Ankara Bilkent City Hospital, Children's Hospital, Department of Pediatric Immunology and Allergy, Ankara, Turkey. [26]Medical University of Vienna, Department of Pediatrics and Adolescent Medicine, Vienna, Austria. [27]St. Anna Children's Hospital, Vienna, Austria.
*Corresponding author. Email: kaan.boztug@ccri.at
†Present address: Drug Safety Research and Evaluation, Takeda Pharmaceuticals U.S.A. Inc. Cambridge, MA, USA.
‡Present address: Cancer Pharmacology and Disease Positioning at Boehringer Ingelheim, Vienna, Austria.
§Present address: Department of Chemistry, University of Konstanz, Konstanz, Germany.

INTRODUCTION

Secondary lymphoid organs (SLOs) are strategically localized throughout the body in the form of tonsils, lymph nodes, the spleen, and Peyer's patches (*1*). They act as surveillance centers and provide the specialized microenvironment necessary for the initiation of adaptive immune responses (*2*). Through a complex network of stromal cells, alongside tightly regulated chemical signals, they facilitate the interaction of various immune cell types, culminating in the formation of germinal centers (GCs) where high-affinity antibody-secreting plasma cells and memory B cells are formed (*3*).

Patients with inborn errors of immunity (IEIs), such as BTK (*4*), RAG1, and RAG2 (*5*) deficiencies, can present with nonpalpable lymph nodes. However, in these cases, the stromal compartment develops normally, and the lymph node structures are formed, although they are not populated by lymphocytes. After successful hematopoietic stem cell transplantation (HSCT), these lymph nodes can organize and function properly (*6*).

Still, there are rare cases of IEIs with aberrant SLO development beyond defects in lymphocytic compartments. Patients deficient in nuclear factor κB (NF-κB)–inducing kinase (NIK) exhibit lymph node aplasia (*7*), whereas 40*S* ribosomal protein SA (RPSA) deficiency is characterized by isolated congenital asplenia (*8*). NIK is ubiquitously expressed and hence directly influences lymphocyte function and development, whereas RPSA deficiency does not affect lymph node architecture or other lymphoid organs beyond the spleen (*7*, *8*). As far as we are aware, no isolated defect causing IEI by disrupting the stromal architecture of SLOs has been described (*9*).

NF-κB is a family of transcription factors with critical roles ranging from the coordination of immune and inflammatory responses in both innate and adaptive immune systems to the development and maintenance of lymphoid organs (*10*). Several receptors can activate NF-κB signaling in immune cells, including the T cell receptor (TCR),

B cell receptor (BCR), Toll-like receptors, and members of the tumor necrosis factor (TNF) superfamily (*10*). The lymphotoxin beta receptor (LTβR), a member of the TNF superfamily, is primarily expressed by stromal cells, such as endothelial, mesenchymal, and epithelial cells, as well as by myeloid cells, including dendritic cells (DCs) and macrophages (*11*, *12*). In contrast, its two ligands, lymphotoxin (LT) and TNF superfamily member 14 (TNFSF14/LIGHT), are predominantly expressed on activated lymphocytes and lymphoid tissue inducer cells (*11*, *13*). These inducer cells have been demonstrated to be required for lymph node formation during embryonic development in mice (*14*). Upon ligand binding, LTβR activates both the canonical NF-κB pathway and, to a greater extent, the noncanonical NF-κB pathway (*15*). The pivotal role of LTβR in the development and regulation of the immune system, through tight communication between stromal cells and lymphocytes, has been established in murine models where its absence (*16*) or inhibition (*17*) results in absent lymph nodes and Peyer's patches, as well as impaired splenic architecture. However, the role of LTβR signaling in humans has remained poorly defined. Here, we report an IEI caused by biallelic loss-of-function (LOF) mutations affecting LTβR and reveal the distinct role of LTβR signaling governing stromal cell function in shaping the microarchitecture and immunological functions of SLOs in humans previously unappreciated in murine studies.

RESULTS

An IEI with lymph node and tonsil aplasia and splenic defect

We studied three male patients (P1 to P3) from two unrelated consanguineous families (Fig. 1A) who had recurrent upper and lower respiratory tract infections starting 4 to 6 months after birth, predominantly of bacterial etiology and requiring intravenous antibiotic treatment. At the age of 3 years, P1 experienced meningitis caused by *Streptococcus pneumoniae* and recovered completely. P2 had an episode of acute hepatitis at the age of 9 years. No causative agent was identified, and a liver biopsy revealed biliary destruction (fig. S1A). We detected an accumulation of $CD4^+$ T cells and B cells as well as some $CD8^+$ T cells in the patient's biopsy, reminiscent of lymphoid infiltrates observed in studies of $Ltbr^{-/-}$ mice (*16*, *18*). After antibiotic treatment and cholecystectomy, the patient no longer exhibited symptoms of acute hepatitis. The older brother of P3 had similar disease manifestations and succumbed to disease complications, including pulmonary hypertension and cor pulmonale, at 18 years of age. Despite the recurrent infections, lymphadenopathy was not detected in any of the patients, and physical examination was remarkable for absent tonsils and nonpalpable lymph nodes. Clinical histories are summarized in Table 1 and supplemental patient clinical histories.

Lymphoscintigraphy in P1 to P3 showed complete lymph node aplasia despite normal lymphatic duct development (Fig. 1B and fig. S1B). The spleen had normal dimensions and morphology on ultrasonographic examination, but Howell-Jolly bodies in peripheral blood smears indicated severe functional hyposplenism (Fig. 1C and fig. S1C) (*19*). In addition, expression of CD47, a signal used by cells to protect themselves from splenic removal by macrophages and DCs (*20*), was decreased on lymphocytes from P1 to P3, further highlighting the impaired splenic function observed in patients with LTβR deficiency (Fig. 1D).

Laboratory studies revealed low levels of immunoglobulin A (IgA) and IgG in P1 to P3 (Table 1). IgM levels were below the age-adjusted normal range in P1 and P2, but normal in P3. After a clinical diagnosis of combined immunodeficiency, regular intravenous immunoglobulin (IVIG) substitution and antibiotic prophylaxis were initiated in P1 to P3, reducing exacerbations of respiratory tract infections. P1 tested DNA positive for genus β human papillomavirus type 24 (HPV-24) (Fig. 1E), which is associated with epidermodysplasia verruciformis and skin cancer (*21*). No other persistent viral infections were observed (Table 1 and supplemental patient clinical histories). Collectively, these results reveal an error of immunity with complete lymph node and tonsil aplasia and splenic defect.

Biallelic germline *LTBR* mutations resulting in loss of expression and impaired noncanonical NF-κB signaling

Given the enigmatic disease etiology, we performed whole-exome sequencing (WES) of P2 and P3 (fig. S2 and tables S1 to S4) and uncovered rare homozygous variants in the *lymphotoxin beta receptor* (*LTBR*) gene, segregating with the disease under the assumption of autosomal recessive inheritance (Fig. 1A and fig. S3A). The *LTBR* variant in P1 and P2 introduces a premature stop codon in exon 1 (c.91C>T, p.Gln31Ter), and P3 carries a missense variant in exon 4 (c.359G>C, p.Arg120Pro), located in a loop of the second cysteine-rich domain (fig. S3B) and predicted to destabilize the protein because of steric clashes of the substituting proline residue (fig. S3C). The identified variants were either absent or ultrarare in public databases (allele frequency < 0.00001), consistent with *LTBR* constraint metrics—a measure for negative selection based on the observed variation/expected variation ratio—hinting at intolerance to both missense and LOF variation. In silico predictions suggested a likely deleterious effect of these variants (table S5).

Serum analysis of P1 and P2 showed a decrease in B lymphocyte chemoattractant (CXCL13/BLC), a chemokine that is highly expressed in SLOs, where it controls the navigation of B cells (Fig. 1F and fig. S4, A to C) (*22*, *23*). CXCL13 is secreted after LTβR activation (*24*), and its reduction has been used as a serum biomarker of successful LTβR inhibition in clinical trials of LTβR antagonists (*25*, *26*). Dermal fibroblasts of P1 to P3 showed complete absence of LTβR protein expression (Fig. 1G). Upon binding its ligand LT, LTβR activates the noncanonical NF-κB pathway, during which the precursor p100 is processed into the active p52 form (*15*). Accordingly, treatment of patient-derived fibroblasts with LT failed to upregulate p52 (Fig. 1H and fig. S5A). In contrast, canonical NF-κB pathway activation induced by TNF-α remained intact (fig. S5B). Correction of the stop-gain variant in fibroblasts of P1 and P3 using CRISPR-Cas9 restored both LTβR expression and LT-induced p100 processing into p52 (Fig. 1, G and H, and fig. S5, A and C). Thus, these results demonstrate that the variants were LOF and causative of the observed, aberrant noncanonical NF-κB signaling.

Deficiency of memory B cells and regulatory and T_{FH} cells

Serial laboratory analyses for P1 to P3 revealed normal ranges of total leukocyte and lymphocyte counts (Table 1). Despite LTβR being absent in B and T lymphocytes (*11*, *12*, *27*) and given that terminal B cell maturation occurs mainly in SLOs, we hypothesized that B cell differentiation may be impaired (*3*). Correspondingly, despite normal total numbers of $CD19^+$ B cells, we detected a significant reduction in GC-like B cells (Fig. 2A), as well as a near absence of both class-switched and unswitched memory B cells (Fig. 2B and fig. S6) and IgA^+ or IgG^+ B cells (fig. S7A). Expansion of T-$bet^{high}CD21^{low}$ B cells is a hallmark of chronic activation of the

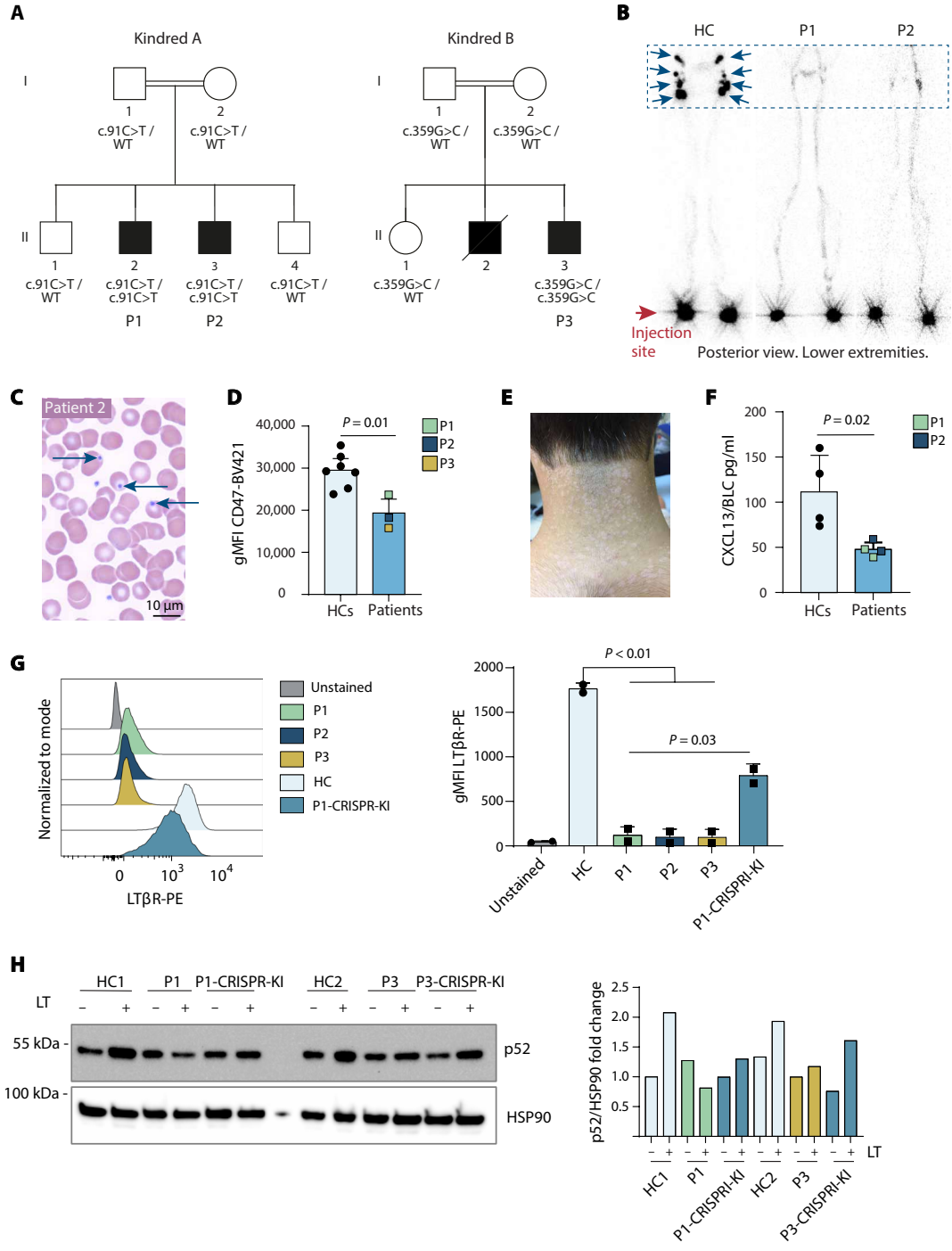

Fig. 1. Identification of patients with LTβR deficiency. (**A**) Pedigrees of the two unrelated families included in this study. Black solid symbols indicate affected individuals. Genotypes are indicated below the symbols. Squares indicate male family members, and circles female family members. Slashed symbols indicate that the individual has died. Roman numerals indicate generations, and Arabic numbers indicate individuals within a generation. (**B**) Lymphoscintigraphy images depicting the lower lymphatic system in an HC alongside P1 and P2 (posterior view). P1 and P2 display normal lymphatic duct development but lack inguinal and iliac lymph nodes (blue dashed rectangle). Blue arrows indicate the main lymphatic nodes. The red arrow indicates the injection sites. (**C**) Howell-Jolly bodies (blue arrows) in erythrocytes in a blood smear from P2. (**D**) Geometric mean fluorescence intensity (gMFI) of CD47 in lymphocytes. Data representative of $N = 2$; HCs ($n = 7$) and patients ($n = 3$). Statistical analysis performed on one of these experiments using unpaired *t* test with Welch's correction. (**E**) Innumerous verrucae planae (flat warts) on the neck of P1. (**F**) Serum values for CXCL13 for P1, P2, and controls ($n = 4$) from two separate Luminex multiplex assays (complete results displayed in fig. S4). (**G**) LTβR expression by flow cytometry analysis in fibroblasts from an HC, P1 to P3, as well as in P1-derived fibroblasts where the mutation was reverted to wild-type by CRISPR-Cas9 editing (CRISPR-KI). (**H**) Representative immunoblot displaying the expression of p52 before and after stimulation with the lymphotoxin (LT) ligand in HC-, P1-, and P1-derived CRISPR-KI fibroblasts. Quantification shown as fold change of p52/HSP90 relative to untreated HC1. HSP90 served as a loading control. Unpaired *t* test was used for statistical analysis in (D), (F), and (G).

Table 1. Clinical and immunological features of patients with LTβR deficiency. TREC and KREC reference values based on (*81*). n.d., not detected; n.a., not available; WBC, whole blood cell count; ALC, absolute lymphocyte count; ANC, absolute neutrophil count; ENA, extractable nuclear antigen; LSC, light signal count.

	Patient 1			Patient 2				Patient 3		
LTBR genomic change (HGVS, NC_000012.12)	g.6384449C>T			g.6384449C>T				g.6385266G>C		
LTBR CDS change (HGVS, ENST00000228918.9)	c.91C>T			c.91C>T				c.359G>C		
LTβR protein change (HGVS, ENSP00000228918.4)	p.Gln31Ter			p.Gln31Ter				p.Arg120Pro		
Age (years), sex	26, male			19, male				9, male		
Age (months) at onset	7			3				6		
Age at evaluation (years)	11	17	25	4	8	13	17	6 months	1.5	8
WBC (cells × 10^3/mm^3)	6.1	4.3	7.0	5.7	5.7	4.7	5.8	22.6	12.0	9.8
Normal range	4.5–13.5	4.5–13	4.5–11	5–15.5	4.5–13.5	4.5–13.5	4.5–13	6–17.5	6–17.5	4.5–13.5
ALC (cells × 10^3/mm^3)	2.1	2.1	2.0	4.0	4.0	2.8	2.6	15.0	11.0	2.5
Normal range	1.5–6.5	1.2–5.2	1–4.8	2–8	1.5–6.8	1.5–6.5	1.2–5.2	4–13.5	4–10.5	1.5–6.8
ANC (cells × 10^3/mm^3)	3.6	1.6	4.1	1.4	1.4	1.5	2.7	n.a.	n.a.	n.a.
Normal range	1.5–8.5	1.8–8	1.8–7.7	1.5–8.5	1.5–8	1.5–8.5	1.8–8			
Thrombocyte counts (cells ×10^3/mm^3)	229	218	195	295	315	490	297	n.a.	n.a.	n.a.
Normal range	150–350	150–350	150–350	150–350	150–350	150–350	150–350			
IgA (mg/dl)	<25	10	<27	24	60	4	27	<6.67	<6.67	<6.67
Normal range	(67–433)	(139–378)	(139–378)	(57–282)	(78–383)	(96–465)	(139–378)	(7–123)	(30–307)	(78–383)
IgG (mg/dl)	690	1700*	1060*	558	851	370*	1180*	150	630*	1000*
Normal range	(835–2694)	(913–1884)	(913–1884)	(745–1804)	(764–2134)	(987–1958)	(913–1884)	(304–1231)	(605–1430)	(764–2134)
IgM (mg/dl)	27	31	37	64	<17	n.a.	38	45	50	60
Normal range	(47–484)	(88–322)	(88–322)	(78–261)	(69–387)		(88–322)	(32–263)	(66–228)	(69–387)
IgE (IU/ml)	12	13.4	89	35	5	n.a.	9.72	<5	<5	<5
Normal range	<60	<60	<60	<60	<60		<60	<15	<60	<60
Anti-nuclear antibody	n.a.	n.a.	Negative	n.a.	n.a.	n.a.	Negative	n.a.	n.a.	AMA-M2, Anti-Ku
ENA profile	n.a.	n.a.	Negative	n.a.	n.a.	n.a.	Negative	n.a.	n.a.	n.a.
Anti-thyroid antibody	n.a.	n.a.	Negative	n.a.	n.a.	n.a.	Negative	n.a.	n.a.	Negative
Isohemagglutinin	1/64	1/64	1/8	1/2	n.a.	n.a.	1/2	n.a.	n.a.	n.a.
Normal range	>1/8	>1/8	>1/8	>1/8			>1/8			
TREC (copy number/10^6 cells)	912			572				n.a.		
Normal range (*81*)	Median (min–max): 6620 (1160–19,600)			Median (min–max): 12,600 (1120–36,200)						
KREC (copy number/10^6 cells)	725			520				n.a.		
Normal range (*81*)	Median (min–max): 1940 (1660–15,800)			Median (min–max): 11,335 (1720–61,000)						

(*Continued*)

(*Continued*)

	Patient 1	Patient 2	Patient 3
Anti–IFN-α antibody	n.a.	n.a.	121
Normal range < 1980 LSC			
Anti–IFN-ω antibody	n.a.	n.a.	110
Normal range < 1961 LSC			
Anti–IFN-γ antibody	n.a.	n.a.	78
Normal range < 1516 LSC			

*Patient was on IgRT at time of sampling.

adaptive immune system in certain infections or autoimmune disorders, and these numbers can be aberrant in patients with IEI (*28*). However, both P2 and P3 exhibited similar numbers of T-bet^{high}CD21^{low} B cells compared with healthy controls (HCs) (fig. S7B). After in vitro cytokine stimulation, patient B cells showed normal activation, proliferation, and, in principle, the ability to undergo class-switch into IgA- or IgG-positive cells (fig. S8). To assess the contribution of T cells to B cell dysfunction, we analyzed the T cell compartment and function in patients with LTβR deficiency. Mouse studies demonstrated the role of LTβR signaling in regulating thymic epithelial cells and stromal cells (*18*, *29*). Although P1 and P2 showed lower TCR excision circle (TREC) levels, their total number of T cells were in the normal range (Table 1), and P1 to P3 had proportions of recent thymic emigrants comparable with those of HCs (fig. S9A). Whereas the CD4$^+$ T cell subpopulations were unaffected, P1 and P2 displayed increased CD8$^+$ terminally differentiated effector memory T cells reexpressing CD45RA (TEMRA) (Fig. 2C), which may correlate with chronic antigenic exposure (*30*). T regulatory (T_{reg}) cells and T follicular helper (T_{FH}) cells were significantly reduced in P1 to P3 (Fig. 2, D and E). Murine studies have, thus far, displayed conflicting results regarding the impact of LT on T helper (T_H) cell differentiation (*13*). Whereas LT has been identified as a prototypical cytokine associated with T_H1 cell responses (*31*), observations in mice deficient in LTβR or its ligand have showed elevated levels of T_H1-type cytokines within their spleens and lungs (*32*). Conversely, exposure to *Leishmania major* infection resulted in a propensity toward T_H2 cell polarization in *Ltbr*$^{-/-}$ mice, resulting in an increase in the severity of the systemic infection (*33*). Stimulation of lymphocytes and assessment of cytokine production revealed a significant reduction in interleukin-4 (IL-4)–producing T_H2 cells in P1 to P3, as well as a trend toward lower interferon-γ (IFN-γ)–producing T_H1 and IL-17A–producing T_H17 cells (Fig. 2F). P1 and P2 T lymphocytes exhibited functionality similar to those from HCs across various in vitro functional assays, including assessments of proliferation and activation, and naïve T cell differentiation into T_{reg} cells (fig. S9B and fig. S10).

Single-cell RNA sequencing (scRNA-seq) of lymphocytes of P1 and P2 confirmed the shift in the CD8$^+$ compartment toward effector memory cells and a lower proportion of T_{reg} cells (Fig. 3, A and B, and fig. S11). Among the most differentially down-regulated genes in CD8$^+$ T lymphocytes were *LTB*, encoding for lymphotoxin-β (LT-β), which binds to LT-α to form the main ligand for LTβR, the lymphotoxin heterotrimer LTα1β2 or lymphotoxin alpha2/beta1 (LTα2β1), and *FOS*, which plays a major role in response to antigenic activation (Fig. 3C) (*17*, *34*). Despite a history of recurrent infections in both patients, differential gene expression analysis revealed no overt differences in the expression of genes associated with chronic inflammation and exhaustion pathways (table S6). Clonality analysis via bulk TCR sequencing (Fig. 3D) and scRNA-seq analysis (fig. S12) showed a reduction in the diversity of T cells from P1 and P2; however, this was driven by the expansion of a few clones on a polyclonal background. Together, these findings confirm a phenotypic shift in T cells toward an effector memory population with a constrained clonotype arrangement, suggesting their relatively quiescent state despite repetitive antigenic challenge. The conserved in vitro functions of patient lymphocytes in contrast with altered in vivo differentiation imply that the observed alterations in subpopulation distributions may not stem from an intrinsic defect within lymphocytes themselves but from alterations in the stromal compartments and the SLOs of the patients.

Alterations in the LTβR and TNF network

Having noticed the significant down-regulation of *LTB* expression across multiple CD8$^+$ cell subtypes from P1 and P2 in the scRNA-seq (Fig. 3C), we measured LTB serum levels in P2 and P3, which were significantly lower compared with HCs (Fig. 4B). We then assessed other members of the TNF family as well. Serum analysis showed a modest increase in TNF-α in P1 and P2 (Fig. 4A and fig. S13A), as well as TNF-β (the soluble homotrimer of LT-α) in P1 (Fig. 4A). TNF superfamily member 14 (TNFSF14/LIGHT), the other known ligand of LTβR, was also elevated in a multiplex analysis of serum from P1 and P2 (Fig. 4A), which was further confirmed via enzyme-linked immunosorbent assay (ELISA) in all three patients (Fig. 4C) (*12*). In addition, Fas ligand (FasL) was also increased in the patients (Fig. 4D). Similar to TNF-α and TNF-β/LTα3 (*35*), both LIGHT (*36*) and FasL (*37*) can also induce apoptosis. Furthermore, overexpression of LIGHT in mice results in autoimmunity (*38*), and increased levels of LIGHT or FasL are associated with autoimmunity in humans (*39*, *40*). In previous studies, *Ltbr*$^{-/-}$ mice exhibited a phenotype of immune dysregulation characterized by splenomegaly, autoantibody production, and

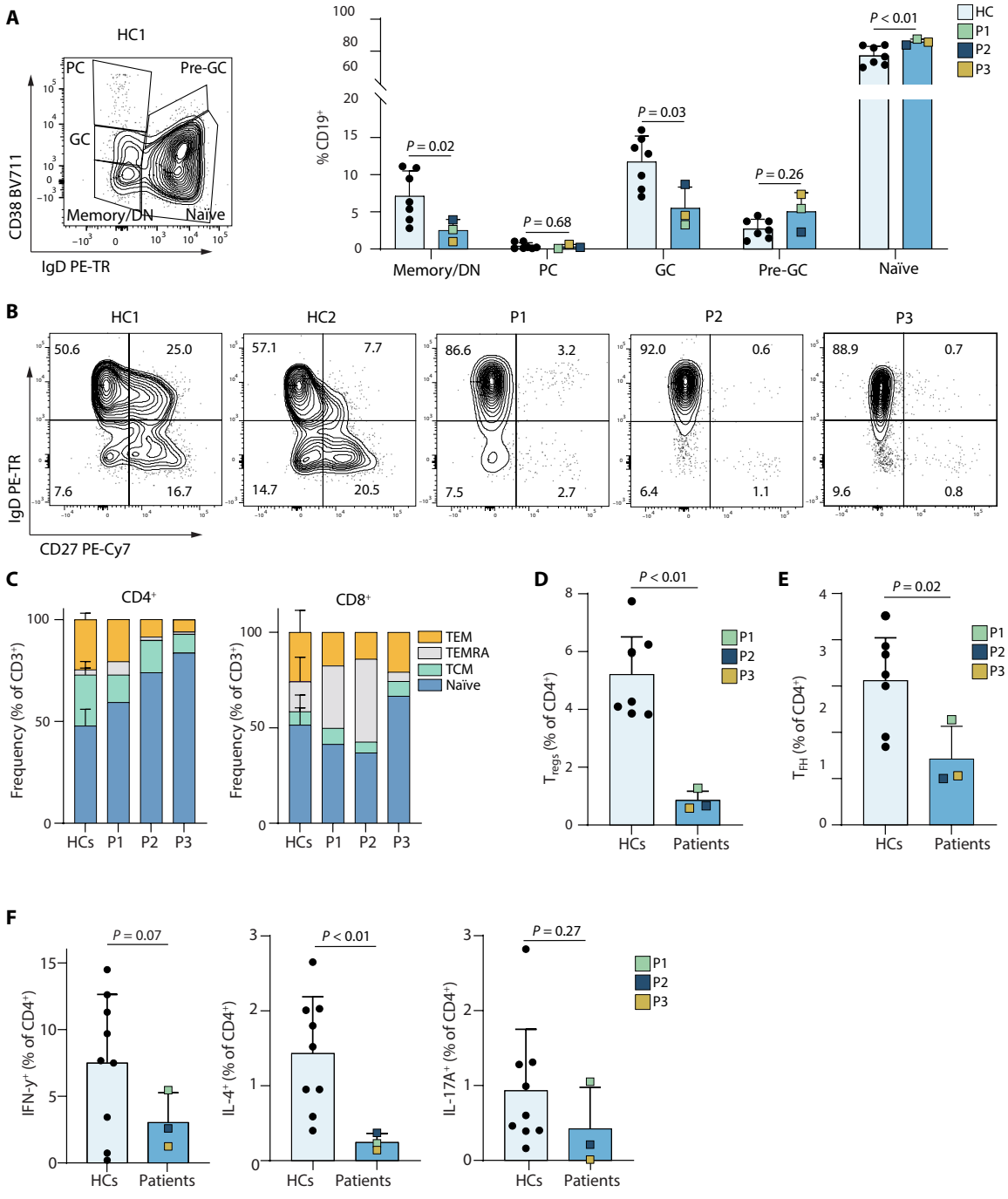

Fig. 2. In-depth characterization of the immune cell compartment from patients with LTβR deficiency. (**A**) Gating strategy to identify subpopulations of $CD19^+$ B cells using flow cytometry and results from patients and HCs ($n = 9$). Subpopulations were classified as plasmablasts, pre-GC, and GC naïve or memory/DN (double-negative). Data shown here are from one experiment, representative of $N = 5$; HCs ($n = 7$) and patients ($n = 3$). (**B**) Representative plots from two HCs and P1 to P3, highlighting the reduction of both class-switched (IgD^-CD27^+) and unswitched (IgD^+CD27^+) $CD19^+$ B cells in the patients. (**C**) Distribution of naïve ($CD45RA^+CCR7^+$), central memory (TCM $CD45RA^-CCR7^+$), terminally differentiated effector memory T cells reexpressing CD45RA (TEMRA $CD45RA^+CCR7^-$), and effector memory (TEM $CD45RA^-CCR7^-$) subpopulations within $CD4^+$ and $CD8^+$ T cell fractions. The data shown here are from one experiment, representative of $N = 4$; HCs ($n = 7$) and patients ($n = 3$). (**D**) Frequency of $CD25^+FOXP3^+$ T_{reg} cells. The data shown here are from one experiment, representative of $N = 2$; HCs ($n = 7$) and patients ($n = 3$). Statistical analysis was performed on one of these experiments. (**E**) Frequency of $CD45RA^-CCR7^-CXCR5^+$ T_{FH} cells. The data shown here are from one experiment, representative of $N = 5$; HCs ($n = 7$) and patients ($n = 3$). Statistical analysis was performed on one of these experiments. (**F**) Distribution of T_H subsets, characterized by cytokine expression on $CD3^+CD4^+CD25^-CD45RA^-$ T cells after 5-hour stimulation with PMA and ionomycin. Results show a shift in the patients from IL-4–producing T_H2 and IL-17–producing T_H17 subsets toward the IFN-γ–producing T_H1 cells (HCs, $n = 10$). The experiment was performed twice with cells from P1 and P2. Statistical analysis was done using ANOVA followed by Bonferroni correction in (A) and unpaired *t* test with Welch's correction in (D) to (F).

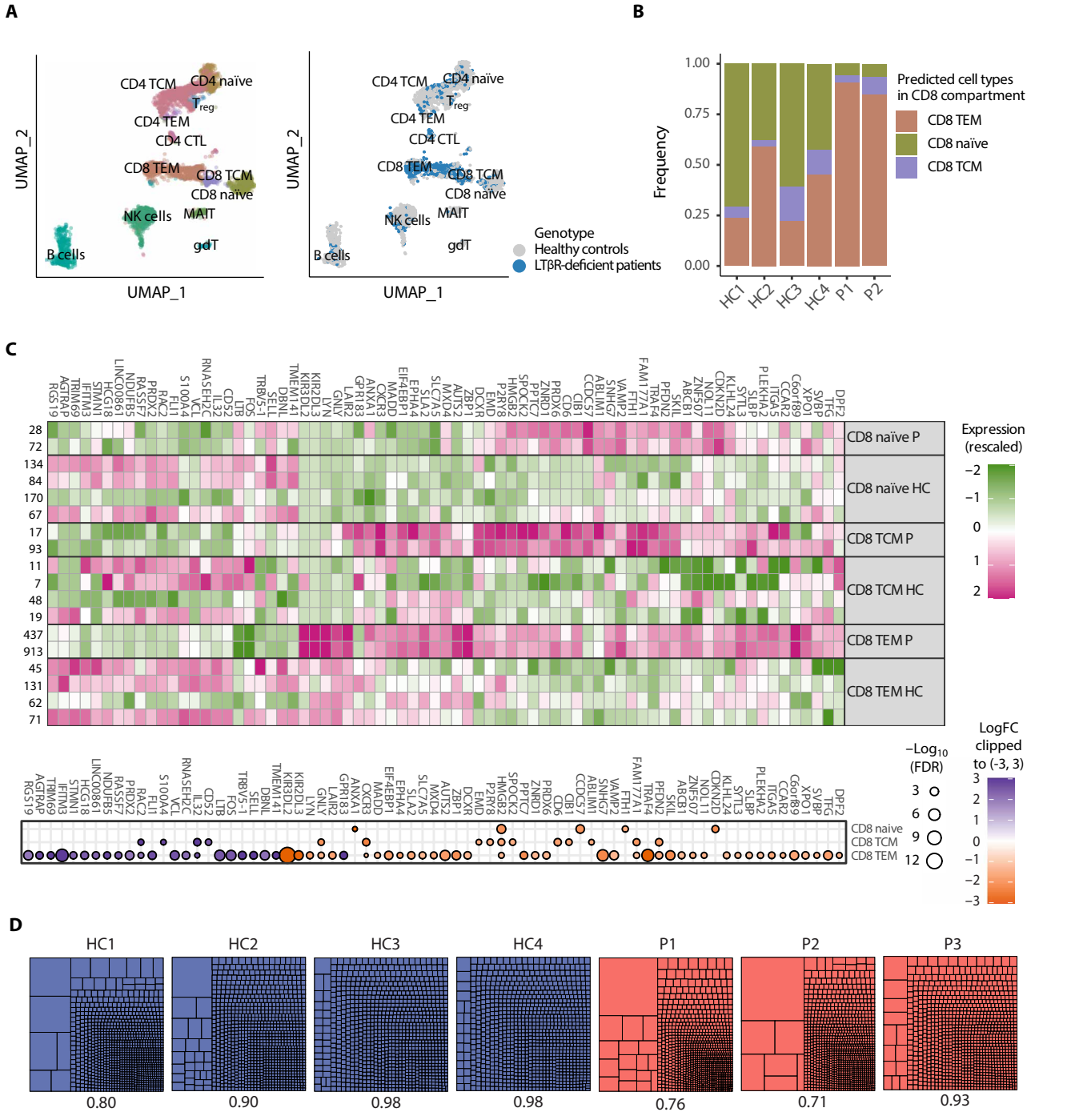

Fig. 3. Sequencing analysis reveals LTB down-regulation and reduced TCR clonality. (**A**) Low-dimensional projection (UMAP plot) of the combined scRNA-seq dataset from P1 and P2 and four HCs. In the left panel, colors correspond to the cell type identified by label transfer from a reference dataset of healthy PBMCs. The right panel displays the same projection, with colors indicating the distribution of patient cells (blue) with the clusters compared with controls (gray). (**B**) Distribution of CD8 T cell compartments in the scRNA-seq data. (**C**) Heatmap showing pseudobulk expression data for genes (shown as columns) that are differentially expressed among P1, P2, and HCs within the $CD8^+$ T cell population (samples and cell types shown as rows). Numbers on the left indicate cell count per group. Dot plots indicate the degree of significance and in which subtypes they were observed. (**D**) TCR clonality results obtained from bulk DNA TCRB sequencing in the 1000 most abundant clones with a productive TCRB VDJ rearrangement and Shannon's evenness indices below each plot.

lymphocytic infiltrates (*16*, *18*, *41*). None of the patients in our cohort had clinically overt autoimmunity or autoinflammation. We screened the patients with extensive autoantibody detection panels, which were negative in P1 and P2. However, P3 tested positive for anti-Ku and anti-mitochondrial antibodies (AMA-M2) despite normal serum liver and renal parameters (Table 1), implying that the presence of these

autoantibodies has not resulted in any clinical manifestations or organ-related disease in this patient to date. Although autoantibodies against type I IFNs have recently been reported in several monogenic IEIs affecting the noncanonical NF-κB pathway (*42*), we could not detect these antibodies in serum from P3 (Table 1).

In addition, increased levels of decoy receptor 3 (DcR3/TNFRSF6B) were observed in the patient's serum compared with those in HCs (Fig. 4E and fig. S13B). DcR3 is a soluble protein with anti-inflammatory properties, acting through the inhibition of both LIGHT and FASL (*43*, *44*). Unexpectedly, we were also able to detect DcR3 in various samples of commercially available IVIG products (Fig. 4D and fig. S13, B and C). Furthermore, we observed that IVIG treatment of a patient with an IEI resulted in increased DcR3 serum levels (fig. S13C). Previous studies have linked DcR3 production to

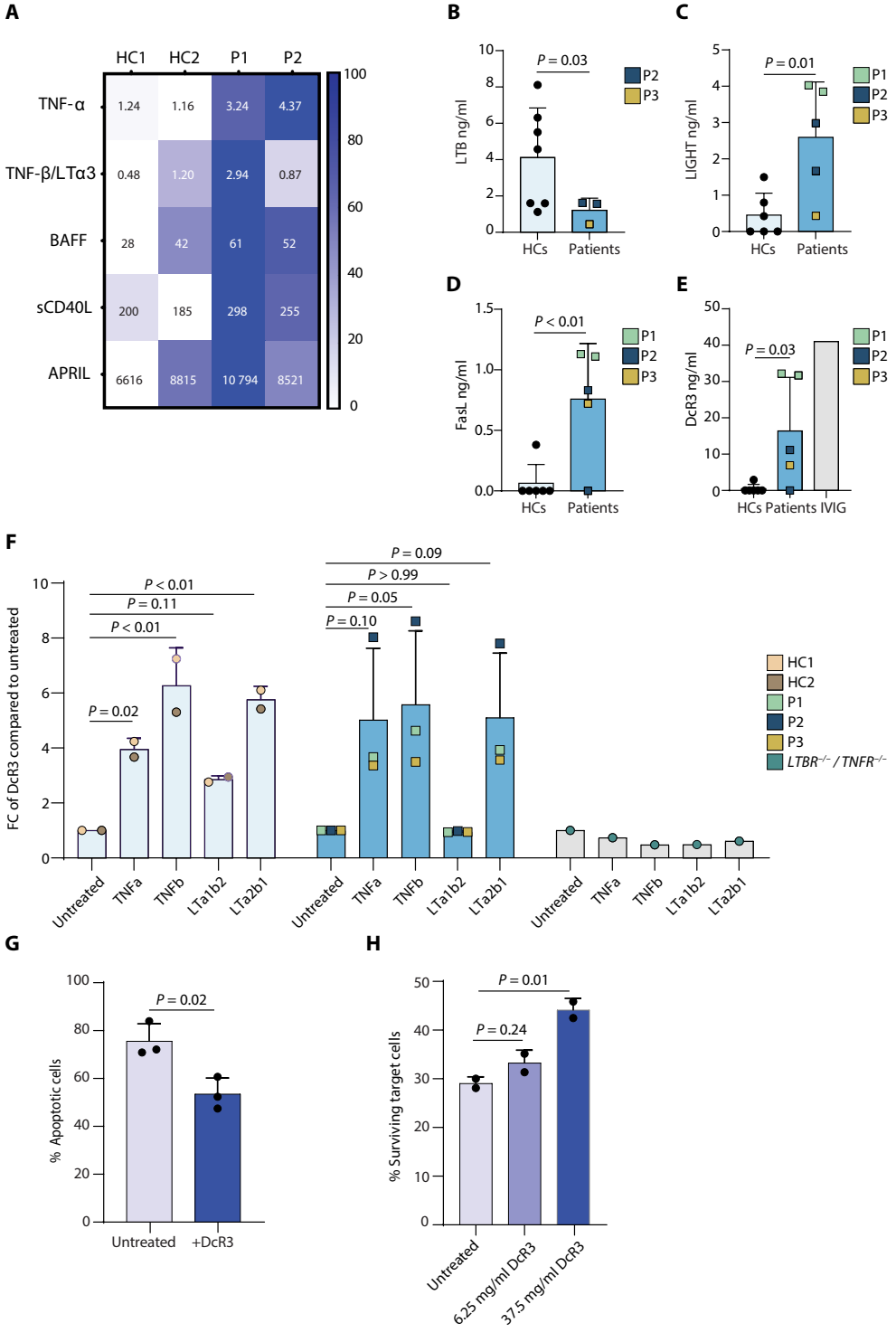

Fig. 4. Alterations in the LTβR/TNF network and the immunomodulatory effect of DcR3. (**A**) Heatmap depicting LEGENDplex multiplex assay for serum samples from P1 and P2 compared with HCs ($n = 2$). Results were individually normalized, with the lowest value set to 0 and the highest value set to 100. All other values were scaled proportionally between these two extremes. Numbers shown are absolute values in picogram per milliliter. (**B**) ELISA serum analysis for LTB. Data are from one experiment with HCs ($n = 7$) and from P2 ($n = 2$) and P3 ($n = 1$). (**C** to **E**) ELISA results for LIGHT/TNFSF14 (C), FasL (D), and DcR3 (E) for serum samples from HCs ($n = 6$) and samples pooled from P1 and P2, from two blood draws, and one from P3. In (E), commercially available IVIG was also tested. Samples from P1 and P2 were taken from two time points. (**F**) ELISA results of DcR3 fold change in treated fibroblasts normalized to untreated cells for HCs ($n = 2$), patients ($n = 3$), and cells from P2 where TNFR1 was knocked out. Each data point represents the average of $N = 2$. (**G**) AICD after restimulation of feeder-expanded T cells with soluble anti-CD3 (sCD3). Graph representing the percentage of apoptotic cells with or without DcR3 treatment. Dots represent average of individual healthy donors ($n = 3$) over two independent experiments. (**H**) Effect of DcR3 treatment on the killing capacity of expanded T cells based on percentage of surviving cocultured p815 target cells treated with sCD3 (0.1 μg/ml) compared with the results in the same condition without the addition of sCD3. Data are representative of two independent experiments, including two of the HCs repeated as a biological replicate. Statistical analysis performed on one of these experiments. Analysis in (B) was performed using unpaired *t* test with Welch's correction. Analysis in (C) to (E) and (G) was performed using unpaired *t* test. Analysis in (F) and (H) was performed using ANOVA followed by Dunnett's post hoc test for multiple comparisons.

PI3K/NF-κB activation (*45*). Treatment of dermal fibroblasts with either TNF-α or TNF-β/LTα3 resulted in the secretion of DcR3 (Fig. 4F), as did treatment with the two known isoforms of lymphotoxin, LTα1β2 and LTα2β1. This effect was dependent on TNFR1 and LTβR stimulation, respectively, because fibroblasts from P2 with an additional TNFR1 knockout showed no response to any of the ligands. Whereas LTα2β1 is capable of binding both receptors, LTα1β2 binds exclusively to LTβR (*46*). Subsequently, LTα1β2 had no effect on patient-derived fibroblasts, whereas LTα2β1 was also able to induce DcR3 production comparably to that of HCs. To assess the immune modulatory function of DcR3, we treated feeder-expanded T cells with DcR3, which protected the T cells from activation-induced cell death (AICD) (Fig. 4G) and reduced the potency of their effector functions such as cytotoxic killing (Fig. 4H). Although the encoding gene is present in the human genome, there is no ortholog in mice (*43*). Collectively, these data demonstrate dysregulation of several members of the TNF superfamily in patients with LTβR deficiency.

Ex vivo coculture reveals functional B cell activation and differentiation

To further characterize the B cell compartment in patients with LTβR deficiency, we performed BCR sequencing and analyzed the somatic hypermutation (SHM) rate in the Ig heavy-chain variable regions (*IGHV*). Whereas the B cell repertoire diversity was comparable between the patients and HCs, indicating that the process of V-D-J recombination and the ability to generate mature naïve B cells is intact in the patients, we observed a significant reduction in the number of mutations in the *IGHV* regions and the percentage of individual B cell clones in which SHM occurred (Fig. 5A and fig. S14, A and B), further corroborating the lack of an efficient GC reaction. Although LTβR signaling is critical for SLO development (*17*, *27*), its direct role in GC formation is less clear (*12*). Established assays to measure B cell differentiation use cytokine stimulation instead of direct cell-cell interactions. We devised an ex vivo model to study the ability of different cell types to interact and induce B cell differentiation to mimic the GC reaction (fig. S15, A to C). We cocultured different combinations of peripheral blood mononuclear cells (PBMCs), DCs, and dermal fibroblasts with or without additional stimulation of a vaccine for measles, mumps, and rubella (MMR) in a transwell system. The DCs were differentiated ex vivo from monocytes and then activated with polyinosinic:polycytidylic acid (poly I:C) (fig. S15B). The dermal fibroblasts were either donor derived or modified by generating *BM2*$^{-/-}$ fibroblasts to inhibit human leukocyte antigen I (HLA-I) expression and prevent T cell–mediated apoptosis (fig. S15C). After the coculture, B cells from HCs, despite some level of variability, showed an up-regulation of the activation marker CD25 as well as activation-induced cytidine deaminase (AID), the enzyme initiating SHM (Fig. 5B) (*47*).

Despite the absence of LTβR signaling, patient B cells were able to differentiate into CD27^{+} memory B cells when coculturing lymphocytes with activated monocyte-derived DCs and stromal cells (Fig. 5C and fig. S16). The additional stimulation with the MMR vaccine induced the differentiation into GC-like (IgD^{-}CD38^{+}) B cells (Fig. 5C and fig. S16). Hence, LTβR deficiency does not result in an intrinsic B cell defect.

Together, these data suggest that LTβR signaling, although critical for SLO development, becomes redundant for B cell differentiation in a GC-like setting if immune cells and stromal cells are brought into close proximity artificially. Therefore, the observed humoral defects in patients with LTβR deficiency may stem from the absence of a conducive environment typically provided by the stromal compartment in SLOs.

DISCUSSION

SLOs play a crucial role in initiating the adaptive immune response and establishing immune memory. Although the formation and organization of SLOs remain active areas of research, LTβR signaling has been identified as a key factor in lymph node development in mice. However, its relevance to humans has been less clear. In this study, we identify LTβR deficiency as the underlying cause of a previously unknown combined immunodeficiency, characterized by a distinct absence of functional SLOs, resulting in hypogammaglobulinemia and low memory B cell levels. The T cell compartment alterations are likely contributing to the observed susceptibility to viral infections, including β-HPV (*21*, *48*).

Although the observed defects in the SLOs are consistent with previously published *Ltbr*$^{-/-}$ mouse models (*12*, *16*, *49*), other key signs of immune dysregulation observed in mice (*18*, *41*, *50*) were not as prominent in patients with LTβR deficiency. We speculate that the defect in the SLOs and subsequently aberrated B cell differentiation and activation may, paradoxically, protect patients from developing and sustaining autoantibody-producing plasma cells. All three patients have been receiving IgG substitution, which is a well-established immune replacement therapy for various autoimmune disorders (*51*), despite its heterogeneity and unclear composition (*52*). We detected increased levels of the DcR3 protein in serum samples at different time points throughout disease progression in all three patients. DcR3 is a protein that has previously been reported to be anti-inflammatory and antiapoptotic via blockade of FasL and LIGHT (*53*), in line with the increased survival and decreased killing activity shown in our study. Intriguingly, DcR3 is not encoded in mice (*43*, *44*). In addition to confirming the immunoregulatory function of DcR3 on human T lymphocytes, we detected high concentrations of DcR3 in various commercially available IVIG solutions. Therefore, it is possible that the increase of DcR3 in patients with LTβR deficiency is in part due to the imbalance of several TNF members or the IVIG replacement therapy. Further delineation of a potential role of DcR3 in modulating immune dysregulation will require additional studies in the future.

The TNF superfamily receptors, particularly RANK, CD40, and LTβR, play crucial roles in the formation of the thymic microenvironment and the induction of central tolerance (*54*). The RANK and CD40 signaling pathways are essential for the development of medullary thymic epithelial cells (mTECs) and the expression of the autoimmune regulator (AIRE), a master regulator of ectopic peripheral antigen expression (*55*). AIRE is vital for negative selection by promoting the expression of peripheral tissue-restricted antigens (TRAs) in mTECs, thereby preventing autoimmunity by ensuring self-tolerance. Mutations in *AIRE* lead to autoimmune polyendocrinopathy candidiasis ectodermal dystrophy, a monogenic disorder characterized by multiorgan autoimmune destruction with a distinct IFN-γ–mediated inflammatory signature (*56*). In contrast, although the LTβR signaling pathway is also necessary for normal thymic architecture and mTEC differentiation, it does not influence AIRE expression or AIRE-dependent TRA expression. Instead, LTβR signaling induces the transcriptional regulator FEZF2, which governs the expression of a distinct set of TRAs (*54*). In LTβR-deficient mice, FEZF2-dependent TRA

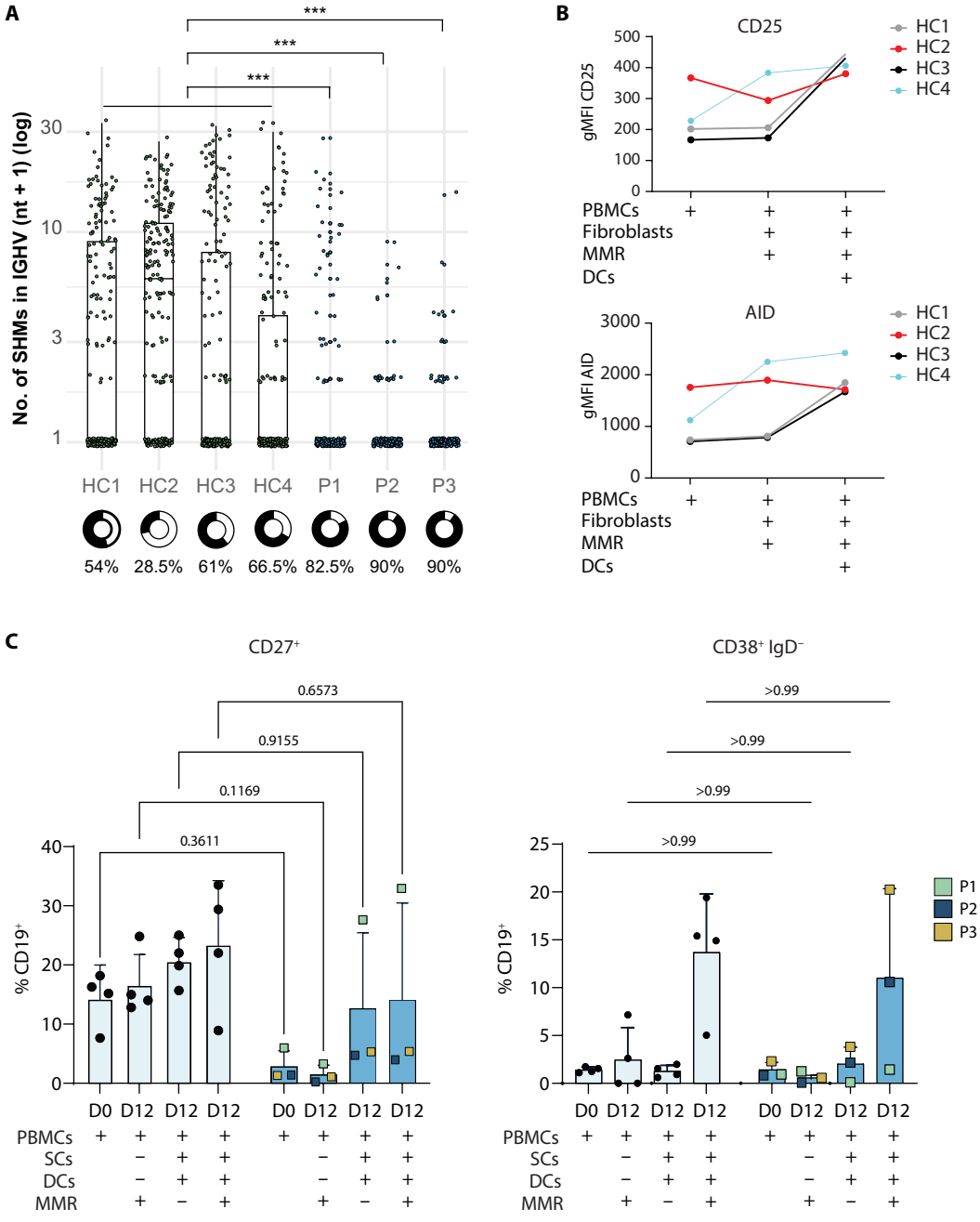

Fig. 5. Functional ex vivo B cell activation in LTβR-deficient cells. (**A**) The rate of SHM in the *IGHV* of the top 200 B cell clones with productive IGH rearrangements. Each dot represents a unique B cell clone with the number of mutated nucleotides (nt) plus one on the *y* axis (logarithmic scale). The percentage of clones with no SHM is shown below each sample in a circular plot. Asterisks represent *P* values <0.001 of Dunnett's test comparison between individual patient samples and the aggregate of HC samples. (**B**) Up-regulation of the activation marker CD25 and AID in $CD19^+$ B cells from HCs ($n = 4$) after 7 days of coculture in various combinations of PBMCs, SCs, DCs, and MMR vaccine as indicated in the panel. (**C**) Differentiation of $CD19^{+s}$ B cells from controls ($n = 4$) and patients into $CD27^+$ memory or $CD38^+IgD^-$ GC-like B cells after 12 days of coculture. Measurements were compared with day 0. Indicated conditions include the addition of stromal cells (SCs), monocyte-derived DCs, or additional treatment with an MMR vaccine. All conditions were stimulated with BAFF every other day. Readout was performed using flow cytometry.

expression is reduced in mTECs, highlighting an alternative pathway for TRA expression independent of AIRE, which implies that LTβR signaling supports the maintenance of thymic stromal cell subsets and chemokine production, playing a broader role in the regulation of the thymic microenvironment. Consistent with this distinct downstream transcriptional impact, the clinical phenotype of patients with LTβR deficiency is quite different from that of AIRE deficiency (*56*), presenting predominantly as B cell dysfunction without the IFN-γ–mediated chronic inflammation and autoimmunity.

Not only $Ltbr^{-/-}$ mice but also mice overexpressing the LTβR ligands LT or LIGHT can exhibit signs of autoimmunity (*39*, *57*), likely to be caused by the unregulated formation of tertiary lymphoid

organs (TLOs) (*58*). These are ectopic lymphoid structures that arise temporarily in proximity to sites of chronic inflammation and resemble SLOs in their organization, function, and dependence on LTβR signaling (*58*). Despite their role as gatekeepers and as a favorable prognostic factor in cancer, TLOs are associated with increased tissue damage in autoimmune diseases (*58*). Thus, LTβR signaling has been a therapeutic target in autoimmune diseases, including rheumatoid arthritis or Sjögren's syndrome, but clinical trials using inhibitors for LTβR (*25*) or its ligand (*26*) have been unsuccessful. The results from our ex vivo GC model suggest that once the process of GC formation has been initiated in either SLOs or TLOs, blockade of LTβR may not suffice to stop the ongoing GC reaction and production of autoantibody-secreting plasma cells.

Our study shows that biallelic LOF mutations in *LTBR* cause an IEI with a predominantly humoral immune deficiency and milder T cell defects, in contrast with murine models where the role for LTβR signaling in autoimmunity was demonstrated by controlling thymic stroma and intestinal microbiota (*59*). Further corroborated by murine data, the nonlymphocyte lineage–specific expression of LTβR suggests that allogeneic HSCT may not provide a curative treatment for human LTβR deficiency (*12*), whereas anti-infective prophylaxis using IVIG and prophylactic antibiotics is imperative. Our study advances our understanding of LTβR as a critical factor of human immune homeostasis, with implications for potential targeted therapies in the context of severe infections and autoimmunity. Whether the observed increase in DcR3 modulates the clinical phenotype warrants further research, and to refine therapeutic strategies, a more profound comprehension of human-specific molecular regulation and tissue specificity in lymphotoxin signaling is paramount. Another limitation of our study—similar to other studies identifying genetic etiologies of rare diseases—is the relatively low numbers of patients identified with this genetic defect, implying that future studies with additional affected individuals will enable the delineation of the full phenotypic spectrum of disease and potential genotype-phenotype correlations.

MATERIALS AND METHODS

Study design

The objective of this study was to investigate the role of LTβR in human immune homeostasis. For this purpose, we performed an array of functional and multiomic experiments on primary material from the patients carrying a germline-encoded homozygous mutation in *LTBR*, after genetic analysis. Furthermore, we made use of cellular models to investigate the effects of the *LTBR* mutation on the function of lymphocytes and stromal cells using biochemical and proteomic approaches. This included a self-developed coculture system of different immune and stromal cells to assess their interaction and capacity to stimulate B cell differentiation. Control samples were used either from healthy shipment controls or taken from healthy local donors.

Study oversight

The study was approved by the relevant institutional review boards and performed in accordance with the guidelines of good clinical practice and the current version of the Declaration of Helsinki. Written informed consent was obtained from the patients or the patients' legal representatives.

Patient and human cell lines

PBMCs from the patients and HCs were isolated via Ficoll gradient. Patient- and HC-derived T cells were expanded by stimulation of PBMCs with irradiated feeder cells, phytohemagglutinin (PHA; 1 μg/ml, Sigma-Aldrich), and IL-2 (100 IU/ml, Novartis) in RPMI 1640 medium containing 5% human serum (IBJB – Inst. Biotechnologies J.BOY, 201021334) and supplemented with 1 mM sodium pyruvate (Thermo Fisher Scientific, 11360039), minimum essential medium nonessential amino acid solution (Sigma-Aldrich, M7145), penicillin (50 U/ml), streptomycin (50 mg/ml), and 10 mM Hepes. Fibroblasts were isolated from skin biopsies from patients and HCs and cultured in Dulbecco's modified Eagle's medium (DMEM) containing 10% fetal calf serum (FCS), penicillin (50 U/ml), streptomycin (50 mg/ml), and 10 mM Hepes. All cells were cultured at 37°C in a humidified atmosphere with 5% CO_2.

Whole-exome sequencing

Genomic DNA (gDNA) was isolated from peripheral blood samples using commercial extraction kits [P2: DNeasy Blood and Tissue Kit (Qiagen); P3: GenEx Blood (GeneAll)]. WES of P2 involved library preparation and exome enrichment using Nextera Rapid Capture Exome kit (Illumina), followed by 150–base pair (bp) paired-end sequencing on the Illumina HiSeq3000 system. Sequenced DNA reads were mapped to the human reference genome (GRCh38/hg38 assembly) by means of the Burrows-Wheeler Aligner (*60*). After variant calling with the Genome Analysis Toolkit HaplotypeCaller (*61*), variant effect predictor was used for annotating single-nucleotide variants and small insertions/deletions (*62*). From the obtained variant calls, nonsynonymous (nonsense, missense, small insertions, and deletions) and splice-region variants (±8 bp from the intron/exon boundaries) were then filtered to exclude those with a minor allele frequency > 0.01 in gnomAD v2.1.1 (*63*).

An in-house database including sequencing data from >1200 individuals was used to further exclude recurrent variants with an allele frequency > 0.02. The remaining variants were prioritized on the basis of literature research and their combined annotation dependent depletion pathogenicity prediction score (*64*).

For P3, the WES library was prepared using the Nextera DNA Prep with Enrichment Kit (Illumina), and sequencing was performed with 150-bp paired-end reads on the Illumina NextSeq 550 platform. Data processing, including mapping, variant calling, and annotation, was conducted with the SEQ Platform v8 (Genomize).

Sanger sequencing

Isolation and purification of gDNA from the probands and family members of both kindreds was performed from peripheral blood using the DNeasy Blood and Tissue Kit (Qiagen). Sanger sequencing was used for the validation and segregation of the *LTBR* variants identified via WES in the patients and their family members. Specific primers were designed to amplify the genomic regions encompassing each of the two identified variants. Sanger sequencing primers used for validation and segregation

of *LTBR* variants in the patient and family members are shown in table S7.

Protein structure visualization

The three-dimensional (3D) structural model of wild-type LTβR was obtained from AlphaFold and visualized with PyMOL (Molecular Graphics System, version 2.0 Schrödinger LLC) (*65*, *66*). MISSENSE3D was used to predict possible effects of p.Arg120Pro on the protein (*67*, *68*).

CRISPR-Cas9 editing of human cells

For the reconstitution experiments, dermal fibroblasts derived from P1 and P3 were edited using CRISPR-Cas9 to reexpress LTβR. Cells were collected and resuspended in Opti-MEM (Thermo Fisher Scientific, 31985062). For electroporation, 10^6 cells were used per condition. Before electroporation, 125 pmol of Cas9 protein (IDT, Alt-R S.p. Cas9 Nuclease V3) and 150 pmol of single gRNA were mixed and incubated for 15 min at room temperature. Subsequently, 100 pmol of single-stranded oligodeoxynucleotide (ssODN) template was added to the cells (table S8). A NEPA21 electroporator (NepaGene) was used for electroporation with the following settings: poring pulse: 250 V, 2.5-ms pulse length, total of two pulses with 50-ms interval between the pulses, 10% decay rate with + polarity; transfer pulse: 20 V, 50-ms pulse length, total of five pulses with 50-ms intervals between the pulses, 40% decay rate with ± polarity. Next, the cells were seeded in DMEM supplemented with 10% FCS. Ten days later, the cells were stained with LTβR antibody and sorted using a fluorescence-activated cell sorting (FACS) Aria Fusion cell sorter. Positive cells were used for further analysis.

For the coculture experiments, dermal fibroblasts from an HC were edited using CRISPR-Cas9 to knock out B2M to prevent expression of HLA-I. Except for the addition of an ssODN template, the electroporation was performed the same way as described above. Afterward, the cells were seeded in DMEM supplemented with 10% FCS. Ten days later, the cells were stained with HLA-I antibody and sorted using an FACS Aria Fusion cell sorter. Negative cells were used for further analysis. Dermal fibroblasts from P2 were used and processed for TNFR1 knockout the same way.

Flow cytometry

PBMCs, either fresh or cryopreserved in liquid nitrogen, were used for immunophenotyping. To reduce unspecific antibody binding, the cells were blocked in RPMI 1640 containing 10% FCS for at least 1 hour before surface staining with antibodies (listed in table S9) for 30 min in the dark at 4°C. Stained cells were acquired with an LSR-Fortessa (BD Biosciences) or FACSymphony (BD Biosciences). FlowJo v10 was used to analyze the data, and Prism v.8 (GraphPad) was used to produce graphs. For intracellular staining, the cells were permeabilized after surface staining with BD 1× Perm/Wash buffer before additional staining with intracellular antibodies for 30 min in the dark at 4°C. The complete list of antibodies used in this study is shown in table S9.

T cell activation and proliferation assay

Feeder-expanded T cells from patients and HCs were stained with violet proliferation dye (VPD450, BD Biosciences) and seeded on 96-well U-shaped plates at 400,000 cells per well in 100 μl of RPMI 1640 supplemented with 10% FCS. The cells were stimulated with either soluble anti-CD3 (sCD3, clone: OKT3; 1 μg/ml), a combination of sCD3 (1 μg/ml) with soluble anti-CD28 (sCD3/CD28, 1 μg/ml, eBioscience), PHA (5 μg/ml, Peprotech), CD3/CD28 DynaBeads (Beads, Invitrogen), or left untreated. Activation was assessed after 24 hours using flow cytometry. Proliferation was measured after 4 days of stimulation by diluting the VPD450.

T_{reg} cell differentiation assay

The T_{reg} cell differentiation assay was used according to the to the manufacturer's protocol (CellXVivo Human T_{reg} Cell Differentiation Kit #CDK006) with small adaptations. In brief, cryopreserved PBMCs from HCs and patients were thawed, and naïve T cells were isolated via magnetic bead separation (Miltenyi, 130-097-095). From each donor, 50,000 cells were either resuspended with RPMI 1640 complete supplemented with 10% FCS or treated using human T_{reg} differentiation medium as prepared using the manufacturer's instructions. Treated cells were then seeded into a 96-well ELISA plate that had been coated with anti-CD3 (clone: OKT3) for 24 hours, whereas the untreated cells were added to uncoated wells. Differentiation of T_{reg} cells was measured after 5 days of cultivation using flow cytometry.

T_H cell cytokine production assay

Cryopreserved PBMCs from patients and HCs were thawed and seeded on 96-well U-shaped plates at 300,000 to 500,000 cells per well in RPMI 1640 supplemented with 10% FCS. Cells were stimulated with 200 nM phorbol 12-myristat 13-acetat (PMA, Sigma-Aldrich) and ionomycin (1 μg/ml, Sigma-Aldrich) or left untreated for a total of 6 hours. After 1 hour of stimulation, brefeldin-A (BioLegend) was added to the cells. Cells were stained with surface antibodies before fixation and stained with intracellular cytokine antibodies. Cells were analyzed using flow cytometry.

B cell activation and proliferation and class switch assay

Cryopreserved PBMCs from P1, P2, and HCs were thawed and stained with violet proliferation dye (VPD450, BD Biosciences) before being seeded on 96-well U-shaped plates at 400,000 cells per well in 100 μl of RPMI 1640 supplemented with 10% FCS. The cells were stimulated with either IL-4 (100 ng/ml, Peprotech) + CD40L (200 ng/ml, Peprotech), IL-21 (20 ng/ml, Peprotech) + CD40L (200 ng/ml), CpG (50 nM, InvivoGen), or left untreated. Activation was assessed after 24 hours using flow cytometry. Proliferation was measured after 6 days of stimulation by diluting the VPD450. Class switch was measured after 5 days of stimulation by $CD19^+$ B cells expressing IgA or IgG.

B cell differentiation assay

Cryopreserved PBMCs from patients and HCs were thawed, and B cells were isolated via magnetic bead separation (Miltenyi 130-101-638). Cells were seeded in 96-well U-shaped plates at 50,000 cells per well in 100 μl of RPMI 1640 supplemented with 10% FCS. The cells were stimulated with a combination of 5 μg of unconjugated goat anti-human F(ab)2 fragments (the Jackson Laboratory), IL-21 (50 ng/ml, Peprotech), CD40L (1 μg/ml, Peprotech), and CpG (1 μg/ml, Peprotech), or left untreated. Differentiation was measured after 6 days of stimulation using flow cytometry.

Stimulation of dermal fibroblasts for DcR3 production

Dermal fibroblasts from HCs, patients, and P2 where TNFR1 was knocked out using the CIRSPR-Cas9 system were seeded at 15,000 cells per well in 200 μl in 48-well plates. After 24 hours, the cells were stimulated with human TNF-α (100 ng/ml, Miltenyi), human TNF-β/LTα3 (200 ng/ml, Peprotech), human LTα1β2 (200 ng/ml, R&D Research), or human LTα2β (200 ng/ml, R&D Research), or left untreated. After 24 hours, the supernatant was collected and used for DcR3 analysis using ELISA (R&D Systems). Results from two independent experiments were averaged before each sample was normalized to its untreated result, followed by pooling of the data of HCs and patients.

Effect of DcR3 on AICD in T cells

Before being washed with phosphate-buffered saline (PBS), 96-well U-shaped plates were coated with CD3 (clone OKT3, 2 μg/ml) overnight at 4°C. After 10 days of feeder stimulation with IL-2 (Novartis) and PHA, expanded T cells from HCs and from P2 were seeded at 100,000 cells per well and treated with DcR3 (3.75 μg/ml, MedChemExpress) or left untreated. After 24 hours of stimulation, the cells were harvested, apoptosis was assessed via staining with annexin V–allophycocyanin (APC) (BD Biosciences), and propidium iodide (BioLegend), and readout was performed using flow cytometry.

Effect of DcR3 on T cell killing function

GFP^+ P815 target cells were treated with anti-CD3 (1 μg/ml, clone: OKT3) antibody for 1 hour or left untreated. Expanded T cells from two HCs previously stimulated for 10 days with feeder cells, IL-2 (Novartis), and PHA were assessed for $CD4^+$ and $CD8^+$ ratio before treatment for 1 hour with DcR3 (6.25 μg/ml, MedChemExpress) or DcR3 (37.5 μg/ml) or left untreated. P815 cells were washed before being cocultured with the expanded T cells at a 1:1 ratio in 96-well U-shaped plates. Aphidicolin (0.2 μg/ml, Sigma-Aldrich) was added to inhibit proliferation of the cells. After 6 hours of coculture, the cells were harvested, and the killing function of T cells was estimated by measuring the number of 7-AAD–negative (BD Biosciences) P815 cells by flow cytometry.

Coculture for B cell differentiation

For the coculture, different combinations of PBMCs, DCs, and fibroblasts were combined with or without additional stimulation of a vaccine for MMR (Merck Sharp und Dohme). PBMCs from patients and HCs were thawed and $CD14^+$ monocytes isolated using CD14 MicroBeads (Miltenyi). Monocytes were then differentiated to DCs over 6 days by adding IL-4 (1000 IU/ml, Peprotech) and granulocyte-macrophage colony-stimulating factor (1000 IU/ml, Peprotech). DCs were stimulated by adding poly I:C (10 μg/ml, InvivoGen) for 24 hours. CRISPR-Cas9–edited *B2M* knockout fibroblasts or patient-derived fibroblasts were seeded at 5000 cells per well into a 24-well transwell. The next day, the donor-specific PBMCs were added at 300,000 cells per well together with donor-specific DCs at 30,000 cells per well with or without addition of 5 μl of MMR per well. RPMI 1640 (1 ml) supplemented with 10% FCS was added in the transwell below. Cells were stimulated with B cell–activating factor (BAFF; 50 ng/ml, Peprotech) every other day. Cells were harvested on day 7 for activation readout or on day 12 for differentiation readout using flow cytometry.

NF-κB stimulation in fibroblasts

For canonical NF-κB activation, dermal fibroblasts were stimulated with human TNF-α (20 ng/ml, Miltenyi) for 10 to 60 min followed by immunoblot analysis. For noncanonical NF-κB activation, dermal fibroblasts were stimulated with human LTα1β2 (200 ng/ml, R&D Research) for 6 hours followed by immunoblot analysis.

Immunoblot

Cell lysates of HC and patient fibroblasts were prepared in radioimmunoprecipitation assay buffer containing protease and phosphatase inhibitor cocktail (Thermo Fisher Scientific). Protein concentrations were determined using the DC Protein Assay Kit II (Bio-Rad), and 20 μg of protein was used and resolved by reducing SDS–polyacrylamide gel electrophoresis with 4 to 15% mini-protean TGX precast protein gels, followed by transfer to polyvinylidene difluoride (PVDF) membranes using the Trans-Blot Turbo RTA Mini 0.45-μm LF PVDF Transfer Kit and the Trans-Blot Turbo transfer system (Bio-Rad). Then, membranes were blocked in 5% bovine serum albumin (BSA) solution for 1 hour at room temperature and subsequent incubation with primary antibodies NF-κB2 p100/p52 (Cell Signaling Technology) and heat shock protein 90 (HSP90) α/β (Santa Cruz Biotechnology) or with phospho–NF-κB p65 (Cell Signaling), IκBα (Cell Signaling Technology), and HSP90α/β (Santa Cruz Biotechnology) overnight at 4°C. Subsequently, membranes were washed three times in tris-buffered saline with Tween 20 detergent (TBST) and incubated with peroxidase-conjugated secondary antibodies for 1 hour at room temperature followed by washing three times in TBST and visualized using chemiluminescence with the ECL Prime Western blot detection reagent (Cytiva) and the ChemiDoc MP imaging system (Bio-Rad).

Enzyme-linked immunosorbent assay

LTB, TNF-α, CXCL13/BLC, DcR3/TNFRSF6B, FasL/TNFSF6, and LIGHT/TNFSF14 levels were detected using ELISA (LTB: catalog no. A312081, Antibodies.com; TNF-α: catalog no. 10737663, Thermo Fisher Scientific; CXCL13/BLC: catalog no. 15444963, Thermo Fisher Scientific; DcR3: catalog no. 15405163, Thermo Fisher Scientific; FasL: catalog no. DY126, DuoSet kit R&D Systems; LIGHT: catalog no. DY664, DuoSet kit, R&D Systems), Luminex Multiplex Assay (Thermo Fisher Scientific) and LEGENDplex (catalog no. 741182, Biolegend) in HC and patient serum samples according to the manufacturer's instructions. Fifty microliters of each serum sample in duplicates was used in all assays.

scRNA sequencing

Samples from P1 and P2 were analyzed along with those from four HCs as previously described (*69*). In brief, cryopreserved PBMCs from the two patients and four HCs were thawed, washed in RPMI 1640 medium, and resuspended in sterile PBS with 0.04% BSA. A single-cell suspension was obtained by passing 1 million cells into a 5-ml FACS tube through a cell strainer and sorting for the live lymphocytes and monocytes on the basis of the forward and side scatter using the FACSAria Fusion (BD). scRNA-seq was then performed on the live samples using the Chromium Single Cell Controller and Chromium Next GEM Single Cell 5' Kit v2 (10x Genomics, Pleasanton, CA) according to the manufacturer's protocol. TCR sequences were enriched at the cDNA stage using the respective reagents, in accordance with the instructions of the VDJ Kit workflow by 10x

Genomics. Sequencing was performed using the Illumina NovaSeq platform in the 75-bp paired-end configuration.

CellRanger v5.0.1 software (10x Genomics) was used for demultiplexing and alignment to the GRCh38-2020-A human reference transcriptome. The R statistics software was used to analyze the processed data. Briefly, CellRanger outputs (filtered count matrices) were further filtered to exclude cells with more than 15% mitochondrial counts or with numbers of detected genes either fewer than 300 or unusually high (per-sample z-score > 2.5). Cell types were annotated using Seurat (v 4.1.0) with sctransform (*70*) normalization (v.0.3.3) and Azimuth (v 0.4.3) (*71*). The reference used was human PBMC annotation level 2. Cells with an annotation score or mapping score less than 0.5 were excluded from further analysis. For visualization, the Azimuth reference space [Uniform Manifold Approximation and Projection (UMAP)] was used, and cell types with fewer than 20 cells annotated (cDC2, pDC, CD16 mono, platelet, HSPC, ILC, and dnT) were excluded. Clonality analysis of the TCR repertoires was based on cells that were assigned exactly one alpha chain CDR3 and one beta chain CDR3. A clonotype was defined as a unique combination of these CDR3 motifs, and clonality for patients and cell types was calculated as 1 minus normalized entropy as done in other studies (*72*). scRNA-seq differential expression (DE) testing of patients versus HCs was done using edgeR (*73*) (v 3.36, default parameters, exact test) and pseudobulk profiles (aggregated counts per patient) to minimize false discoveries (*74*). Each test was filtered to exclude genes with false discovery rate (FDR)–adjusted P value >0.05; the remaining genes were ordered by P value. Several tests were performed, each focusing on different cell populations. Tests were performed within $CD8^+$ T cells (aggregating CD8 naïve, CD8 TCM, and CD8 TEM) and within the individual $CD8^+$ cell types. Expression heatmaps show normalized expression (DESeq2 vst function after aggregating counts of all cells per group) z-scored per gene and cropped to the range of −2 to 2. Genes selected for display in the heatmaps had to have P value rank ≤ 45 and logFC rank ≤ 45 (grouped by fold-change direction) in one of the CD8 cell type DE tests. After differential gene expression analysis, we performed gene set enrichment analysis using hypergeometric tests. For the tests, we considered all the genes retained by edgeR as background, whereas the DE genes (FDR ≤ 0.05) were considered the genes of interest. The following genes defined the "exhaustion" gene set: *PDCD1*, *CTLA4*, *NFATC1*, *SPRY2*, *BATF*, *VHL*, *FOXO1*, *FOXP1*, *LAG3*, *CD244*, *CD160*, *HAVCR2*, *TRAF1*, *TNFRSF9*, *IL10RA*, *IL10*, *PRDM1*, *STAT3*, *IFNA1*, *IFNB1*, *IL21*, *CXCR5*, *SOCS3*, *GATA3*, *IKZF2*, *BCL6*, *BCL2*, *TBX21*, and *EOMES*. A significant enrichment for exhaustion was not observed in any of the DE test results (P values >0.1).

BCR and TCR sequencing

For BCR and TCR sequencing, DNA was isolated from PBMCs or whole blood of patients and HCs. The DNA used for BCR sequencing of P1 and P2 was isolated from B cell–enriched samples using magnetic cell sorting separation as described previously in the B cell differentiation protocol. Sequencing was performed using protocols and primers standardized by the EuroClonality-NGS Working Group and sequenced with the Illumina MiSeq v3 600-sequencing kit (MS-102-3003) with 20% PhiX v3 Control library (FC-110-3001; both Illumina, San Diego, CA, USA) following the manufacturer's instructions (*75*, *76*). Demultiplexed sequencing data were analyzed using the ARResT/Interrogate platform to annotate individual clones for further processing with R (*77*, *78*). For the analysis of clonality, only productively rearranged IGH and TCRB clones were included in the analysis, and only the top 1000 clones by frequency were included for the figure plots and diversity calculations. For the analysis of the SHM rate, all productively rearranged IGH clones with a unique amino acid sequence in the CDR3 and with a coverage of at least five reads in the sample were used, and its representative sequence with the highest number of reads was used for alignment. The alignment to the *IGHV* gene reference sequences was performed using the IMGT/HighV-QUEST platform, and the resulting files were processed using custom R code to generate statistics and plots (*79*, *80*). The number of nucleotide mutations was calculated for each clone with a productive IGH rearrangement in the CDR1, CDR2, FR2, and FR3 regions of the rearrangement. For the figure plots and underlying statistics, the top 200 clones by their frequency were analyzed for each sample. A detailed analysis of the *IGHV3-23* gene was performed for all clones with a productive rearrangement of this *IGHV* gene, and a mutational rate was calculated for each amino acid position on the basis of the alignment to the IMGT reference. A mutational rate is shown as a median per position for all four HCs with an error bar corresponding to the 75th percentile and individual values per position for all patients.

Statistical analysis

For individual comparisons of independent groups, the Student's t test was performed. Welch's correction was used if the two groups had unequal variances or sample sizes. For multiple comparisons, a one- or two-way analysis of variance (ANOVA) was applied, followed by Bonferroni post hoc test to correct for multiple comparisons. In the case of multiple comparisons toward one dataset (e.g., untreated), Dunnet's post hoc test was used instead. Data graphs and analyses were made using PRISM software (GraphPad Software Inc.), and error bars display the SDs.

Supplementary Materials

The PDF file includes:
Materials
Figs. S1 to S16
Tables S1 to S9
References (*82*–*85*)

Other Supplementary Material for this manuscript includes the following:
Data file S1
MDAR Reproducibility Checklist

REFERENCES AND NOTES

1. H. L. Horsnell, R. J. Tetley, H. De Belly, S. Makris, L. J. Millward, A. C. Benjamin, L. A. Heeringa, C. M. de Winde, E. K. Paluch, Y. Mao, S. E. Acton, Lymph node homeostasis and adaptation to immune challenge resolved by fibroblast network mechanics. *Nat. Immunol.* **23**, 1169–1182 (2022).
2. P. C. de Casas, K. Knopper, R. D. Sarkar, W. Kastenmuller, Same yet different - How lymph node heterogeneity affects immune responses. *Nat. Rev. Immunol.* **24**, 358–374 (2024).
3. G. D. Victora, M. C. Nussenzweig, Germinal Centers. *Annu. Rev. Immunol.* **40**, 413–442 (2022).
4. D. Vetrie, I. Vorechovsky, P. Sideras, J. Holland, A. Davies, F. Flinter, L. Hammarstrom, C. Kinnon, R. Levinsky, M. Bobrow, C. I. E. Smith, D. R. Bentley, The gene involved in X-linked agammaglobulinaemia is a member of the src family of protein-tyrosine kinases. *Nature* **361**, 226–233 (1993).
5. A. Villa, L. D. Notarangelo, *RAG* gene defects at the verge of immunodeficiency and immune dysregulation. *Immunol. Rev.* **287**, 73–90 (2019).
6. R. J. O'Reilly, B. Dupont, S. Pahwa, E. Grimes, E. M. Smithwick, R. Pahwa, S. Schwartz, J. A. Hansen, F. P. Siegal, M. Sorell, A. Svejgaard, C. Jersild, M. Thomsen, P. Platz,

P. L'Esperance, R. A. Good, Reconstitution in severe combined immunodeficiency by transplantation of marrow from an unrelated donor. *N. Engl. J. Med.* **297**, 1311–1318 (1977).
7. K. L. Willmann, S. Klaver, F. Dogu, E. Santos-Valente, W. Garncarz, I. Bilic, E. Mace, E. Salzer, C. D. Conde, H. Sic, P. Majek, P. P. Banerjee, G. I. Vladimer, S. Haskologlu, M. G. Bolkent, A. Kupesiz, A. Condino-Neto, J. Colinge, G. Superti-Furga, W. F. Pickl, M. C. van Zelm, H. Eibel, J. S. Orange, A. Ikinciogullari, K. Boztug, Biallelic loss-of-function mutation in *NIK* causes a primary immunodeficiency with multifaceted aberrant lymphoid immunity. *Nat. Commun.* **5**, 5360 (2014).
8. A. Bolze, N. Mahlaoui, M. Byun, B. Turner, N. Trede, S. R. Ellis, A. Abhyankar, Y. Itan, E. Patin, S. Brebner, P. Sackstein, A. Puel, C. Picard, L. Abel, L. Quintana-Murci, S. N. Faust, A. P. Williams, R. Baretto, M. Duddridge, U. Kini, A. J. Pollard, C. Gaud, P. Frange, D. Orbach, J. F. Emile, J.-L. Stephan, R. Sorensen, A. Plebani, L. Hammarstrom, M. E. Conley, L. Selleri, J.-L. Casanova, Ribosomal protein SA haploinsufficiency in humans with isolated congenital asplenia. *Science* **340**, 976–978 (2013).
9. S. G. Tangye, W. Al-Herz, A. Bousfiha, C. Cunningham-Rundles, J. L. Franco, S. M. Holland, C. Klein, T. Morio, E. Oksenhendler, C. Picard, A. Puel, J. Puck, M. R. J. Seppanen, R. Somech, H. C. Su, K. E. Sullivan, T. R. Torgerson, I. Meyts, Human inborn errors of immunity: 2022 update on the classification from the international union of immunological societies expert committee. *J. Clin. Immunol.* **42**, 1473–1507 (2022).
10. S.-C. Sun, The non-canonical NF-κB pathway in immunity and inflammation. *Nat. Rev. Immunol.* **17**, 545–558 (2017).
11. C. F. Ware, T. L. VanArsdale, P. D. Crowe, J. L. Browning, The ligands and receptors of the lymphotoxin system. *Curr. Top. Microbiol. Immunol.* **198**, 175–218 (1995).
12. C. F. Ware, Network communications: Lymphotoxins, LIGHT, and TNF. *Annu. Rev. Immunol.* **23**, 787–819 (2005).
13. V. Upadhyay, Y.-X. Fu, Lymphotoxin signalling in immune homeostasis and the control of microorganisms. *Nat. Rev. Immunol.* **13**, 270–279 (2013).
14. G. Eberl, S. Marmon, M.-J. Sunshine, P. D. Rennert, Y. Choi, D. R. Littman, An essential function for the nuclear receptor RORγ(t) in the generation of fetal lymphoid tissue inducer cells. *Nat. Immunol.* **5**, 64–73 (2004).
15. E. Dejardin, N. M. Droin, M. Delhase, E. Haas, Y. Cao, C. Makris, Z.-W. Li, M. Karin, C. F. Ware, D. R. Green, The lymphotoxin-β receptor induces different patterns of gene expression via two NF-κB pathways. *Immunity* **17**, 525–535 (2002).
16. A. Futterer, K. Mink, A. Luz, M. H. Kosco-Vilbois, K. Pfeffer, The lymphotoxin β receptor controls organogenesis and affinity maturation in peripheral lymphoid tissues. *Immunity* **9**, 59–70 (1998).
17. P. D. Rennert, J. L. Browning, R. Mebius, F. Mackay, P. S. Hochman, Surface lymphotoxin alpha/beta complex is required for the development of peripheral lymphoid organs. *J. Exp. Med.* **184**, 1999–2006 (1996).
18. T. Nitta, M. Tsutsumi, S. Nitta, R. Muro, E. C. Suzuki, K. Nakano, Y. Tomofuji, S. Sawa, T. Okamura, J. M. Penninger, H. Takayanagi, Fibroblasts as a source of self-antigens for central immune tolerance. *Nat. Immunol.* **21**, 1172–1180 (2020).
19. M. V. Lenti, S. Luu, R. Carsetti, F. Osier, R. Ogwang, O. E. Nnodu, U. Wiedermann, J. Spencer, F. Locatelli, G. R. Corazza, A. Di Sabatino, Asplenia and spleen hypofunction. *Nat. Rev. Dis. Primers.* **8**, 71 (2022).
20. B. R. Blazar, F. P. Lindberg, E. Ingulli, A. Panoskaltsis-Mortari, P. A. Oldenborg, K. Iizuka, W. M. Yokoyama, P.-A. Taylor, CD47 (integrin-associated protein) engagement of dendritic cell and macrophage counterreceptors is required to prevent the clearance of donor lymphohematopoietic cells. *J. Exp. Med.* **194**, 541–550 (2001).
21. P. M. Howley, H. J. Pfister, Beta genus papillomaviruses and skin cancer. *Virology* **479–480**, 290–296 (2015).
22. S. A. van de Pavert, B. J. Olivier, G. Goverse, M. F. Vondenhoff, M. Greuter, P. Beke, K. Kusser, U. E. Hopken, M. Lipp, K. Niederreither, R. Blomhoff, K. Sitnik, W. W. Agace, T. D. Randall, W. J. de Jonge, R. E. Mebius, Chemokine CXCL13 is essential for lymph node initiation and is induced by retinoic acid and neuronal stimulation. *Nat. Immunol.* **10**, 1193–1199 (2009).
23. K. M. Ansel, V. N. Ngo, P. L. Hyman, S. A. Luther, R. Forster, J. D. Sedgwick, J. L. Browning, M. Lipp, J. G. Cyster, A chemokine-driven positive feedback loop organizes lymphoid follicles. *Nature* **406**, 309–314 (2000).
24. V. N. Ngo, H. Korner, M. D. Gunn, K. N. Schmidt, D. S. Riminton, M. D. Cooper, J. L. Browning, J. D. Sedgwick, J. G. Cyster, Lymphotoxin α/β and tumor necrosis factor are required for stromal cell expression of homing chemokines in B and T cell areas of the spleen. *J. Exp. Med.* **189**, 403–412 (1999).
25. E. W. S. Clair, A. N. Baer, C. Wei, G. Noaiseh, A. Parke, A. Coca, T. O. Utset, M. C. Genovese, D. J. Wallace, J. McNamara, K. Boyle, L. Keyes-Elstein, J. L. Browning, N. Franchimont, K. Smith, J. M. Guthridge, I. Sanz, J. A. James, E. Autoimmunity, Centers of clinical efficacy and safety of baminercept, a lymphotoxin β receptor fusion protein, in primary sjogren's syndrome: Results from a phase II randomized, double-blind, placebo-controlled trial. *Arthritis Rheumatol.* **70**, 1470–1480 (2018).
26. W. P. Kennedy, J. A. Simon, C. Offutt, P. Horn, A. Herman, M. J. Townsend, M. T. Tang, J. L. Grogan, F. Hsieh, J. C. Davis, Efficacy and safety of pateclizumab (anti-lymphotoxin-α) compared to adalimumab in rheumatoid arthritis: A head-to-head phase 2 randomized controlled study (The ALTARA Study). *Arthritis Res. Ther.* **16**, 467 (2014).
27. S. A. van de Pavert, R. E. Mebius, New insights into the development of lymphoid tissues. *Nat. Rev. Immunol.* **10**, 664–674 (2010).
28. B. Keller, V. Strohmeier, I. Harder, S. Unger, K. J. Payne, G. Andrieux, M. Boerries, P. T. Felixberger, J. J. M. Landry, A. Nieters, A. Rensing-Ehl, U. Salzer, N. Frede, S. Usadel, R. Elling, C. Speckmann, I. Hainmann, E. Ralph, K. Gilmour, M. W. J. Wentink, M. van der Burg, H. S. Kuehn, S. D. Rosenzweig, U. Kolsch, H. von Bernuth, P. Kaiser-Labusch, F. Gothe, S. Hambleton, A. D. Vlagea, A. G. Garcia, L. Alsina, G. Markelj, T. Avcin, J. Vasconcelos, M. Guedes, J. Y. Ding, C. L. Ku, B. Shadur, D. T. Avery, N. Venhoff, J. Thiel, H. Becker, L. Erazo-Borras, C. M. Trujillo-Vargas, J. L. Franco, C. Fieschi, S. Okada, P. E. Gray, G. Uzel, J.-L. Casanova, M. Fliegauf, B. Grimbacher, H. Eibel, S. Ehl, R. E. Voll, M. Rizzi, P. Stepensky, V. Benes, C. S. Ma, C. Bossen, S. G. Tangye, K. Warnatz, The expansion of human T-bet^{high}CD21^{low} B cells is T cell dependent. *Sci. Immunol.* **6**, eabh0891 (2021).
29. A. Borelli, M. Irla, Lymphotoxin: From the physiology to the regeneration of the thymic function. *Cell Death Differ.* **28**, 2305–2314 (2021).
30. A. Salumets, L. Tserel, A. P. Rumm, L. Turk, K. Kingo, K. Saks, A. Oras, R. Uibo, R. Tamm, H. Peterson, K. Kisand, P. Peterson, Epigenetic quantification of immunosenescent CD8$^+$ TEMRA cells in human blood. *Aging Cell* **21**, e13607 (2022).
31. I. Gramaglia, D. N. Mauri, K. T. Miner, C. F. Ware, M. Croft, Lymphotoxin αβ is expressed on recently activated naive and Th1-like CD4 cells but is down-regulated by IL-4 during Th2 differentiation. *J. Immunol.* **162**, 1333–1338 (1999).
32. H.-S. Kang, S. E. Blink, R. K. Chin, Y. Lee, O. Kim, J. Weinstock, T. Waldschmidt, D. Conrad, B. Chen, J. Solway, A. I. Sperling, Y.-X. Fu, Lymphotoxin is required for maintaining physiological levels of serum IgE that minimizes Th1-mediated airway inflammation. *J. Exp. Med.* **198**, 1643–1652 (2003).
33. J. M. Ehrchen, J. Roth, K. Roebrock, G. Varga, W. Domschke, R. Newberry, C. Sorg, C. Muller-Tidow, C. Sunderkotter, T. Kucharzik, T. W. Spahn, The absence of cutaneous lymph nodes results in a Th2 response and increased susceptibility to *Leishmania major* infection in mice. *Infect. Immun.* **76**, 4241–4250 (2008).
34. G. Xiao, A. Deng, H. Liu, G. Ge, X. Liu, Activator protein 1 suppresses antitumor T cell function via the induction of programmed death 1. *Proc. Natl. Acad. Sci. U.S.A.* **109**, 15419–15424 (2012).
35. O. Micheau, J. Tschopp, Induction of TNF receptor I-mediated apoptosis via two sequential signaling complexes. *Cell* **114**, 181–190 (2003).
36. Y. Zhai, R. Guo, T. L. Hsu, G. L. Yu, J. Ni, B. S. Kwon, G. W. Jiang, J. Lu, J. Tan, M. Ugustus, K. Carter, L. Rojas, F. Zhu, C. Lincoln, G. Endress, L. Xing, S. Wang, K. O. Oh, R. Gentz, S. Ruben, M. E. Lippman, S. L. Hsieh, D. Yang, LIGHT, a novel ligand for lymphotoxin beta receptor and TR2/HVEM induces apoptosis and suppresses in vivo tumor formation via gene transfer. *J. Clin. Invest.* **102**, 1142–1151 (1998).
37. D. C. Huang, M. Hahne, M. Schroeter, K. Frei, A. Fontana, A. Villunger, K. Newton, J. Tschopp, A. Strasser, Activation of Fas by FasL induces apoptosis by a mechanism that cannot be blocked by Bcl-2 or Bcl-x(L). *Proc. Natl. Acad. Sci. U.S.A.* **96**, 14871–14876 (1999).
38. J. Wang, J. C. Lo, A. Foster, P. Yu, H. M. Chen, Y. Wang, K. Tamada, L. Chen, Y. X. Fu, The regulation of T cell homeostasis and autoimmunity by T cell-derived LIGHT. *J. Clin. Invest.* **108**, 1771–1780 (2001).
39. C. F. Ware, M. Croft, G. A. Neil, Realigning the LIGHT signaling network to control dysregulated inflammation. *J. Exp. Med.* **219**, e20220236 (2022).
40. C. Giordano, G. Stassi, R. De Maria, M. Todaro, P. Richiusa, G. Papoff, G. Ruberti, M. Bagnasco, R. Testi, A. Galluzzo, Potential involvement of Fas and its ligand in the pathogenesis of Hashimoto's thyroiditis. *Science* **275**, 960–963 (1997).
41. T. Boehm, S. Scheu, K. Pfeffer, C. C. Bleul, Thymic medullary epithelial cell differentiation, thymocyte emigration, and the control of autoimmunity require lympho-epithelial cross talk via LTβR. *J. Exp. Med.* **198**, 757–769 (2003).
42. T. Le Voyer, A. V. Parent, X. Liu, A. Cederholm, A. Gervais, J. Rosain, T. Nguyen, M. P. Lorenzo, E. Rackaityte, D. Rinchai, P. Zhang, L. Bizien, G. Hancioglu, P. Ghillani-Dalbin, J.-L. Charuel, Q. Philippot, M. S. Gueye, M. R. L. M. Renkilaraj, M. Ogishi, C. Soudee, M. Migaud, F. Rozenberg, M. Momenilandi, Q. Riller, L. Imberti, O. M. Delmonte, G. Muller, B. Keller, J. Orrego, W. A. F. Gallego, T. Rubin, M. Emiroglu, N. Parvaneh, D. Eriksson, M. Aranda-Guillen, D. I. Berrios, L. Vong, C. H. Katelaris, P. Mustillo, J. Raedler, J. Bohlen, J. B. Celik, C. Astudillo, S. Winter, NF-κB Consortium, COVID Human Genetic Effort, C. McLean, A. Guffroy, J. L. DeRisi, D. Yu, C. Miller, Y. Feng, A. Guichard, V. Beziat, J. Bustamante, Q. Pan-Hammarstrom, Y. Zhang, L. B. Rosen, S. M. Holland, M. Bosticardo, H. Kenney, R. Castagnoli, C. A. Slade, K. Boztug, N. Mahlaoui, S. Latour, R. S. Abraham, V. Lougaris, F. Hauck, A. Sediva, F. Atschekzei, G. Sogkas, M. C. Poli, M. A. Slatter, B. Palterer, M. D. Keller, A. Pinzon-Charry, A. Sullivan, L. Droney, D. Suan, M. Wong, A. Kane, H. Hu, C. Ma, H. Grombirikova, P. Ciznar, I. Dalal, N. Aladjidi, M. Hie, E. Lazaro, J. Franco, S. Keles, M. Malphettes, M. Pasquet, M. E. Maccari, A. Meinhardt, A. Ikinciogullari, M. Shahrooei, F. Celmeli, P. Frosk, C. C. Goodnow, P. E. Gray, A. Belot, H. S. Kuehn, S. D. Rosenzweig, M. Miyara, F. Licciardi, A. Servettaz, V. Barlogis, G. Le Guenno, V. M. Herrmann, T. Kuijpers, G. Ducoux, F. Sarrot-Reynauld, C. Schuetz, C. Cunningham-Rundles, F. Rieux-Laucat, S. G. Tangye, C. Sobacchi, R. Doffinger, K. Warnatz, B. Grimbacher, C. Fieschi, L. Berteloot,

V. L. Bryant, S. T. Assant, H. Su, B. Neven, L. Abel, Q. Zhang, B. Boisson, A. Cobat, E. Jouanguy, O. Kampe, P. Bastard, C. M. Roifman, N. Landegren, L. D. Notarangelo, M. S. Anderson, J.-L. Casanova, A. Puel, Autoantibodies against type I IFNs in humans with alternative NF-κB pathway deficiency. *Nature* **623**, 803–813 (2023).
43. D. Liang, Y. Hou, X. Lou, H. Chen, Decoy receptor 3 improves survival in experimental sepsis by suppressing the inflammatory response and lymphocyte apoptosis. *PLOS ONE* **10**, e0131680 (2015).
44. S.-C. Weng, M.-C. Wen, S.-L. Hsieh, N.-J. Chen, D.-C. Tarng, Decoy receptor 3 suppresses T-cell priming and promotes apoptosis of effector T-cells in acute cell-mediated rejection: The role of reverse signaling. *Front. Immunol.* **13**, 879648 (2022).
45. D.-Y. Liang, S. Sha, Q. Yi, J. Shi, Y. Chen, Y. Hou, Q. Chang, Hepatitis B X protein upregulates decoy receptor 3 expression via the PI3K/NF-κB pathway. *Cell. Signal.* **62**, 109346 (2019).
46. L. Williams-Abbott, B. N. Walter, T. C. Cheung, C. R. Goh, A. G. Porter, C. F. Ware, The lymphotoxin-α (LTα) subunit is essential for the assembly, but not for the receptor specificity, of the membrane-anchored LTα1β2 heterotrimeric ligand. *J. Biol. Chem.* **272**, 19451–19456 (1997).
47. P. Revy, T. Muto, Y. Levy, F. Geissmann, A. Plebani, O. Sanal, N. Catalan, M. Forveille, R. Dufourcq-Labelouse, A. Gennery, I. Tezcan, F. Ersoy, H. Kayserili, A. G. Ugazio, N. Brousse, M. Muramatsu, L. D. Notarangelo, K. Kinoshita, T. Honjo, A. Fischer, A. Durandy, Activation-induced cytidine deaminase (AID) deficiency causes the autosomal recessive form of the hyper-IgM syndrome (HIGM2). *Cell* **102**, 565–575 (2000).
48. A. El Kettani, F. Ailal, J. El Bakkouri, K. Zerouali, V. Beziat, E. Jouanguy, J.-L. Casanova, A. A. Bousfiha, HPV-related skin phenotypes in patients with inborn errors of immunity. *Pathogens* **11**, 857 (2022).
49. Y. Shou, E. Koroleva, C. M. Spencer, S. A. Shein, A. A. Korchagina, K. A. Yusoof, R. Parthasarathy, E. A. Leadbetter, A. N. Akopian, A. R. Munoz, A. V. Tumanov, Redefining the role of lymphotoxin beta receptor in the maintenance of lymphoid organs and immune cell homeostasis in adulthood. *Front. Immunol.* **12**, 712632 (2021).
50. R. K. Chin, J. C. Lo, O. Kim, S. E. Blink, P. A. Christiansen, P. Peterson, Y. Wang, C. Ware, Y.-X. Fu, Lymphotoxin pathway directs thymic *Aire* expression. *Nat. Immunol.* **4**, 1121–1127 (2003).
51. Z. Yu, V. A. Lennon, Mechanism of intravenous immune globulin therapy in antibody-mediated autoimmune diseases. *N. Engl. J. Med.* **340**, 227–228 (1999).
52. N. Washburn, R. Meccariello, S. Hu, M. Hains, N. Bhatnagar, H. Sarvaiya, B. Kapoor, J. Schaeck, I. Pino, A. Manning, J. C. Lansing, C. J. Bosques, High-resolution physicochemical characterization of different intravenous immunoglobulin products. *PLOS ONE* **12**, e0181251 (2017).
53. K.-Y. Yu, B. Kwon, J. Ni, Y. Zhai, R. Ebner, B. S. Kwon, A newly identified member of tumor necrosis factor receptor superfamily (TR6) suppresses LIGHT-mediated apoptosis. *J. Biol. Chem.* **274**, 13733–13736 (1999).
54. H. Takaba, Y. Morishita, Y. Tomofuji, L. Danks, T. Nitta, N. Komatsu, T. Kodama, H. Takayanagi, Fezf2 orchestrates a thymic program of self-antigen expression for immune tolerance. *Cell* **163**, 975–987 (2015).
55. J. L. Bautista, N. T. Cramer, C. N. Miller, J. Chavez, D. I. Berrios, L. E. Byrnes, J. Germino, V. Ntranos, J. B. Sneddon, T. D. Burt, J. M. Gardner, C. J. Ye, M. S. Anderson, A. V. Parent, Single-cell transcriptional profiling of human thymic stroma uncovers novel cellular heterogeneity in the thymic medulla. *Nat. Commun.* **12**, 1096 (2021).
56. V. Oikonomou, G. Smith, G. M. Constantine, M. M. Schmitt, E. M. N. Ferre, J. C. Alejo, D. Riley, D. Kumar, L. Dos Santos Dias, J. Pechacek, Y. Hadjiyannis, T. Webb, B. A. Seifert, R. Ghosh, M. Walkiewicz, D. Martin, M. Besnard, B. D. Snarr, S. Deljookorani, C. R. Lee, T. DiMaggio, P. Barber, L. B. Rosen, A. Cheng, A. Rastegar, A. A. de Jesus, J. Stoddard, H. S. Kuehn, T. J. Break, H. H. Kong, L. Castelo-Soccio, B. Colton, B. M. Warner, D. E. Kleiner, M. M. Quezado, J. L. Davis, K. P. Fennelly, K. N. Olivier, S. D. Rosenzweig, A. F. Suffredini, M. S. Anderson, M. Swidergall, C. Guillonneau, L. D. Notarangelo, R. Goldbach-Mansky, O. Neth, M. T. Monserrat-Garcia, J. Valverde-Fernandez, J. M. Lucena, A. L. Gomez-Gila, A. Garcia Rojas, M. R. J. Seppanen, J. Lohi, M. Hero, S. Laakso, P. Klemetti, V. Lundberg, O. Ekwall, P. Olbrich, K. K. Winer, B. Afzali, N. M. Moutsopoulos, S. M. Holland, T. Heller, S. Pittaluga, M. S. Lionakis, The role of interferon-γ in autoimmune polyendocrine syndrome type 1. *N. Engl. J. Med.* **390**, 1873–1884 (2024).
57. G. M. Seleznik, J. Zoller, T. O'Connor, R. Graf, M. Heikenwalder, The role of lymphotoxin signaling in the development of autoimmune pancreatitis and associated secondary extra-pancreatic pathologies. *Cytokine Growth Factor Rev.* **25**, 125–137 (2014).
58. Y. Sato, K. Silina, M. van den Broek, K. Hirahara, M. Yanagita, The roles of tertiary lymphoid structures in chronic diseases. *Nat. Rev. Nephrol.* **19**, 525–537 (2023).
59. Y. Zhang, T.-J. Kim, J. A. Wroblewska, V. Tesic, V. Upadhyay, R. R. Weichselbaum, A. V. Tumanov, H. Tang, X. Guo, H. Tang, Y.-X. Fu, Type 3 innate lymphoid cell-derived lymphotoxin prevents microbiota-dependent inflammation. *Cell. Mol. Immunol.* **15**, 697–709 (2018).
60. H. Li, R. Durbin, Fast and accurate long-read alignment with Burrows-Wheeler transform. *Bioinformatics* **26**, 589–595 (2010).
61. R. Poplin, V. Ruano-Rubio, M. A. De Pristo, T. J. Fennell, M. O. Carneiro, G. A. Van der Auwera, D. E. Kling, L. D. Gauthier, A. Levy-Moonshine, D. Roazen, K. Shakir, J. Thibault, S. Chandran, C. Whelan, M. Lek, S. Gabriel, M. J. Daly, B. Neale, D. G. MacArthur, E. Banks, Scaling accurate genetic variant discovery to tens of thousands of samples. bioRxiv 201178 [Preprint] (2017); https://doi.org/10.1101/201178.
62. W. McLaren, L. Gil, S. E. Hunt, H. S. Riat, G. R. S. Ritchie, A. Thormann, P. Flicek, F. Cunningham, The ensembl variant effect predictor. *Genome Biol.* **17**, 122 (2016).
63. K. J. Karczewski, L. C. Francioli, G. Tiao, B. B. Cummings, J. Alfoldi, Q. Wang, R. L. Collins, K. M. Laricchia, A. Ganna, D. P. Birnbaum, L. D. Gauthier, H. Brand, M. Solomonson, N. A. Watts, D. Rhodes, M. Singer-Berk, E. M. England, E. G. Seaby, J. A. Kosmicki, R. K. Walters, K. Tashman, Y. Farjoun, E. Banks, T. Poterba, A. Wang, C. Seed, N. Whiffin, J. X. Chong, K. E. Samocha, E. Pierce-Hoffman, Z. Zappala, A. H. O'Donnell-Luria, E. V. Minikel, B. Weisburd, M. Lek, J. S. Ware, C. Vittal, I. M. Armean, L. Bergelson, K. Cibulskis, K. M. Connolly, M. Covarrubias, S. Donnelly, S. Ferriera, S. Gabriel, J. Gentry, N. Gupta, T. Jeandet, D. Kaplan, C. Llanwarne, R. Munshi, S. Novod, N. Petrillo, D. Roazen, V. Ruano-Rubio, A. Saltzman, M. Schleicher, J. Soto, K. Tibbetts, C. Tolonen, G. Wade, M. E. Talkowski, Genome Aggregation Database Consortium, B. M. Neale, M. J. Daly, D. G. MacArthur, The mutational constraint spectrum quantified from variation in 141,456 humans. *Nature* **581**, 434–443 (2020).
64. M. Kircher, D. M. Witten, P. Jain, B. J. O'Roak, G. M. Cooper, J. Shendure, A general framework for estimating the relative pathogenicity of human genetic variants. *Nat. Genet.* **46**, 310–315 (2014).
65. J. Jumper, R. Evans, A. Pritzel, T. Green, M. Figurnov, O. Ronneberger, K. Tunyasuvunakool, R. Bates, A. Zidek, A. Potapenko, A. Bridgland, C. Meyer, S. A. A. Kohl, A. J. Ballard, A. Cowie, B. Romera-Paredes, S. Nikolov, R. Jain, J. Adler, T. Back, S. Petersen, D. Reiman, E. Clancy, M. Zielinski, M. Steinegger, M. Pacholska, T. Berghammer, S. Bodenstein, D. Silver, O. Vinyals, A. W. Senior, K. Kavukcuoglu, P. Kohli, D. Hassabis, Highly accurate protein structure prediction with AlphaFold. *Nature* **596**, 583–589 (2021).
66. M. Varadi, S. Anyango, M. Deshpande, S. Nair, C. Natassia, G. Yordanova, D. Yuan, O. Stroe, G. Wood, A. Laydon, A. Zidek, T. Green, K. Tunyasuvunakool, S. Petersen, J. Jumper, E. Clancy, R. Green, A. Vora, M. Lutfi, M. Figurnov, A. Cowie, N. Hobbs, P. Kohli, G. Kleywegt, E. Birney, D. Hassabis, S. Velankar, AlphaFold protein structure database: Massively expanding the structural coverage of protein-sequence space with high-accuracy models. *Nucleic Acids Res.* **50**, D439–D444 (2022).
67. T. Khanna, G. Hanna, M. J. E. Sternberg, A. David, Missense3D-DB web catalogue: An atom-based analysis and repository of 4M human protein-coding genetic variants. *Hum. Genet.* **140**, 805–812 (2021).
68. S. Ittisoponpisan, S. A. Islam, T. Khanna, E. Alhuzimi, A. David, M. J. E. Sternberg, Can predicted protein 3D structures provide reliable insights into whether missense variants are disease associated? *J. Mol. Biol.* **431**, 2197–2212 (2019).
69. S. Kostel Bal, S. Giuliani, J. Block, P. Repiscak, C. Hafemeister, T. Shahin, N. Kasap, B. Ransmayr, Y. Miao, C. van de Wetering, A. Frohne, R. Jimenez Heredia, M. Schuster, S. Zoghi, V. Hertlein, M. Thian, A. Bykov, R. Babayeva, S. Bilgic Eltan, E. Karakoc-Aydiner, L. E. Shaw, I. Chowdhury, M. Varjosalo, R. J. Arguello, M. Farlik, A. Ozen, E. Serfling, L. Dupre, C. Bock, F. Halbritter, J. T. Hannich, I. Castanon, M. J. Kraakman, S. Baris, K. Boztug, Biallelic *NFATC1* mutations cause an inborn error of immunity with impaired $CD8^+$ T cell function and perturbed glycolysis. *Blood* **142**, 827–845 (2023).
70. C. Hafemeister, R. Satija, Normalization and variance stabilization of single-cell RNA-seq data using regularized negative binomial regression. *Genome Biol.* **20**, 296 (2019).
71. Y. Hao, S. Hao, E. Andersen-Nissen, W. M. Mauck III, S. Zheng, A. Butler, M. J. Lee, A. J. Wilk, C. Darby, M. Zager, P. Hoffman, M. Stoeckius, E. Papalexi, E. P. Mimitou, J. Jain, A. Srivastava, T. Stuart, L. M. Fleming, B. Yeung, A. J. Rogers, J. M. McElrath, C. A. Blish, R. Gottardo, P. Smibert, R. Satija, Integrated analysis of multimodal single-cell data. *Cell* **184**, 3573–3587.e29 (2021).
72. A. Reuben, J. Zhang, S. H. Chiou, R. M. Gittelman, J. Li, W. C. Lee, J. Fujimoto, C. Behrens, X. Liu, F. Wang, K. Quek, C. Wang, F. Kheradmand, R. Chen, C.-W. Chow, H. Lin, C. Bernatchez, A. Jalali, X. Hu, C.-J. Wu, A. K. Eterovic, E. R. Parra, E. Yusko, R. Emerson, S. Benzeno, M. Vignali, X. Wu, Y. Ye, L. D. Little, C. Gumbs, X. Mao, X. Song, S. Tippen, R. L. Thornton, T. Cascone, A. Snyder, J. A. Wargo, R. Herbst, S. Swisher, H. Kadara, C. Moran, N. Kalhor, J. Zhang, P. Scheet, A. A. Vaporciyan, B. Sepesi, D. L. Gibbons, H. Robins, P. Hwu, J. V. Heymach, P. Sharma, J. P. Allison, V. Baladandayuthapani, J. J. Lee, M. M. Davis, I. I. Wistuba, P. A. Futreal, J. Zhang, Comprehensive T cell repertoire characterization of non-small cell lung cancer. *Nat. Commun.* **11**, 603 (2020).
73. D. J. McCarthy, Y. Chen, G. K. Smyth, Differential expression analysis of multifactor RNA-seq experiments with respect to biological variation. *Nucleic Acids Res.* **40**, 4288–4297 (2012).
74. J. W. Squair, M. Gautier, C. Kathe, M. A. Anderson, N. D. James, T. H. Hutson, R. Hudelle, T. Qaiser, K. J. E. Matson, Q. Barraud, A. J. Levine, G. La Manno, M. A. Skinnider, G. Courtine, Confronting false discoveries in single-cell differential expression. *Nat. Commun.* **12**, 5692 (2021).
75. M. Bruggemann, M. Kotrova, H. Knecht, J. Bartram, M. Boudjogrha, V. Bystry, G. Fazio, E. Fronkova, M. Giraud, A. Grioni, J. Hancock, D. Herrmann, C. Jimenez, A. Krejci,

J. Moppett, T. Reigl, M. Salson, B. Scheijen, M. Schwarz, S. Songia, M. Svaton, J. J. M. van Dongen, P. Villarese, S. Wakeman, G. Wright, G. Cazzaniga, F. Davi, R. Garcia-Sanz, D. Gonzalez, P. J. T. A. Groenen, M. Hummel, E. A. Macintyre, K. Stamatopoulos, C. Pott, J. Trka, N. Darzentas, A. W. Langerak, EuroClonality-NGS working group, EuroClonality, Standardized next-generation sequencing of immunoglobulin and T cell receptor gene recombinations for MRD marker identification in acute lymphoblastic leukaemia; a EuroClonality-NGS validation study. *Leukemia* **33**, 2241–2253 (2019).

76. H. Knecht, T. Reigl, M. Kotrova, F. Appelt, P. Stewart, V. Bystry, A. Krejci, A. Grioni, K. Pal, K. Stranska, K. Plevova, J. Rijntjes, S. Songia, M. Svaton, E. Fronkova, J. Bartram, B. Scheijen, D. Herrmann, R. Garcia-Sanz, J. Hancock, J. Moppett, J. J. M. van Dongen, G. Cazzaniga, F. Davi, P. J. T. A. Groenen, M. Hummel, E. A. Macintyre, K. Stamatopoulos, J. Trka, A. W. Langerak, D. Gonzalez, C. Pott, M. Bruggemann, N. Darzentas, EuroClonality-NGS working group, Quality control and quantification in IG/TR next-generation sequencing marker identification: Protocols and bioinformatic functionalities by EuroClonality-NGS. *Leukemia* **33**, 2254–2265 (2019).
77. V. Bystry, T. Reigl, A. Krejci, M. Demko, B. Hanakova, A. Grioni, H. Knecht, M. Schlitt, P. Dreger, L. Sellner, D. Herrmann, M. Pingeon, M. Boudjoghra, J. Rijntjes, C. Pott, A. W. Langerak, P. Groenen, F. Davi, M. Bruggemann, N. Darzentas, EuroClonality-NGS, ARResT/Interrogate: An interactive immunoprofiler for IG/TR NGS data. *Bioinformatics* **33**, 435–437 (2017).
78. R Core Team, R: A language and environment for statistical computing (2021).
79. X. Brochet, M.-P. Lefranc, V. Giudicelli, IMGT/V-QUEST: The highly customized and integrated system for IG and TR standardized V-J and V-D-J sequence analysis. *Nucleic Acids Res.* **36**, W503–W508 (2008).
80. M.-P. Lefranc, V. Giudicelli, C. Ginestoux, J. Jabado-Michaloud, G. Folch, F. Bellahcene, Y. Wu, E. Gemrot, X. Brochet, J. Lane, L. Regnier, F. Ehrenmann, G. Lefranc, P. Duroux, IMGT, the international ImMunoGeneTics information system. *Nucleic Acids Res.* **37**, D1006–D1012 (2009).
81. G. Senturk, Y. Y. Ng, S. B. Eltan, D. Baser, I. Ogulur, D. Altindirek, S. Firtina, H. Yilmaz, B. Kocamis, A. Kiykim, Y. Camcioglu, M. C. Ar, T. Sudutan, S. Beken, S. G. Temel, Y. Alanay, E. Karakoc-Aydiner, S. Baris, A. Ozen, U. Ozbek, M. Sayitoglu, O. H. Ng, Determining T and B Cell development by TREC/KREC analysis in primary immunodeficiency patients and healthy controls. *Scand. J. Immunol.* **95**, e13130 (2022).
82. L. L. Andersen, N. Mork, L. S. Reinert, E. Kofod-Olsen, R. Narita, S. E. Jorgensen, K. A. Skipper, K. Honing, H. H. Gad, L. Ostergaard, T. F. Orntoft, V. Hornung, S. R. Paludan, J. G. Mikkelsen, T. Fujita, M. Christiansen, R. Hartmann, T. H. Mogensen, Functional IRF3 deficiency in a patient with herpes simplex encephalitis. *J. Exp. Med.* **212**, 1371–1379 (2015).
83. S. Petrovski, Q. Wang, E. L. Heinzen, A. S. Allen, D. B. Goldstein, Genic intolerance to functional variation and the interpretation of personal genomes. *PLOS Genet.* **9**, e1003709 (2013).
84. N. M. Ioannidis, J. H. Rothstein, V. Pejaver, S. Middha, S. K. McDonnell, S. Baheti, A. Musolf, Q. Li, E. Holzinger, D. Karyadi, L. A. Cannon-Albright, C. C. Teerlink, J. L. Stanford, W. B. Isaacs, J. Xu, K. A. Cooney, E. M. Lange, J. Schleutker, J. D. Carpten, I. J. Powell, O. Cussenot, G. Cancel-Tassin, G. G. Giles, R. J. MacInnis, C. Maier, C. L. Hsieh, F. Wiklund, W. J. Catalona, W. D. Foulkes, D. Mandal, R. A. Eeles, Z. Kote-Jarai, C. D. Bustamante, D. J. Schaid, T. Hastie, E. A. Ostrander, J. E. Bailey-Wilson, P. Radivojac, S. N. Thibodeau, A. S. Whittemore, W. Sieh, REVEL: An ensemble method for predicting the pathogenicity of rare missense variants. *Am. J. Hum. Genet.* **99**, 877–885 (2016).
85. University of Michigan; National Heart, Lung, and Blood Institute (NHLBI), NHLBI Trans-Omics for Precision Medicine (TOPMed) Whole Genome Sequencing Program. BRAVO variant browser. (2024) [accessed 27 February 2024].

Acknowledgments: We thank the clinical cooperation partners and the patients and their families for participation in our study; H. Schachner from the Medical University of Vienna (MUW) for providing histologic stains of the biopsy; L. Shaw from the MUW for preparing the library for scRNA-seq; A. Skotnicova and E. Fronkova from the Second Faculty of Medicine, Charles University and University Hospital Motol in Prague, and K. Liszt from the St. Anna Children's Cancer Research Institute Vienna for providing valuable reagents and assistance with BCR and TCR sequencing; and R. Kirnbauer from the MUW for assistance in analyzing the skin biopsy. We would like to thank "Can Sucak Candan Biseyler" Foundation (CSCBF) for support. CSCBF was founded in 2018 to honor C. Sucak, who lost his life because of complications of primary immunodeficiency. CSCBF supports research in the field of primary immunodeficiency and promotes awareness. We would like to express our gratitude to T. Meyer, C. Meisel, and N. Unterwalder from the Department of Immunology at Labor Berlin for assistance in testing material from P3 for IFN autoantibodies. We thank A. Bykov from the St. Anna Children's Cancer Research Institute Vienna for helping to archive the raw sequencing data on the European Genome-Phenome Archive. We thank U. Pötschger, Statistics Team Leader at the St. Anna Children's Cancer Research Institute, for valuable support in the statistical analysis of our data. **Funding:** This work was supported by an European Research Council Consolidator Grant ("iDysChart", grant no. 820074, to K.B.); Austrian Research Promotion Agency (FFG), Research Partnerships programme (B.R.); P.T. Engelhorn Foundation, Postdoctoral Fellowship (C.v.d.W.); Austrian Academy of Sciences, DOC Fellowship (no. 25590) (J.B.); FWF, Lise Meitner Postdoctoral Fellowship (M.J.K.); the Scientific and Technological Research Council of Turkey (318S202) (S.B.); and Alex's Lemonade Stand Foundation for Childhood Cancer (ALSF) 20-17258 (M.F. and F.H.). **Author contributions:** B.R. performed most of the experiments, including flow cytometry, generation of CRISPR-Cas9–edited cells, and the set-up and optimization of coculture experiments; B.R. and S.K.B. interpreted clinical and immunological data; S.K.B. supervised B.R. while performing functional in vitro experiments together; M.T. initiated the project and provided critical initial input; B.R. and M.T. performed the initial immunophenotyping and B cell activation and class-switch assay; M.S. performed the BCR and TCR sequencing and analyzed the data; C.H. analyzed scRNA-seq data under the supervision of F.H. of samples prepared by B.R. and S.K.B., who also helped in the interpretation of the scRNA-seq data; A.K., M.T., A.S.-R., B.E., and Ü.A. analyzed WES data and identified the *LTBR* variants; A.S.-R. and A.K. performed Sanger sequencing validation and segregation analyses; B.R., M.T., and C.v.d.W. performed immunoblotting; B.R. and C.v.d.W. performed ELISA experiments; J.B., M.S., and B.R. performed the T_H subset analysis; A.F. performed the LTβR protein structure visualization; S.B., M.Y.A., A.O., E.K.-A., A.K., S.B.E., O.A., S.K., and S.I. took care of P1 and P2; S.B., M.Y.A., and A.M. collected patient samples and organized their shipment; A.M., G.D.T., and A.C. took care of P3; B.H. analyzed the skin biopsy from P1; M.F. supervised the scRNA-seq; I.S.-K. provided histopathologic evaluation of the biopsy sample from P2 and the blood smears from P1 and P2; H.v.B. assessed interferon autoantibodies in P3; R.P. and S.K. provided technical input; M.J.K., M.R., and A.V.T. provided critical intellectual input; B.R., S.K.B., M.J.K., M.S., C.v.d.W., I.C., and K.B. wrote the manuscript with input from all co-authors; K.B. conceptualized and coordinated the study, provided laboratory resources, and took overall responsibility of the study. All authors vouch for the data and the analysis. All authors approved the final version of the manuscript and agreed to publish the paper. **Competing interests:** The authors declare that they have no competing interests. **Data and materials availability:** Raw sequencing reads are deposited in the European Genome-Phenome Archive [accession numbers EGAS00001007271 (BCR/TCRseq) and EGAS00001007271 (scRNA-seq)]. These data are available via controlled access to safeguard patient privacy. The R code used for the analysis of single-cell RNA-sequencing data is available on GitHub at https://github.com/cancerbits/ransmayr2024_ltbr and for the analysis of the BCR and TCR sequencing results at https://github.com/msvtnCCRI/ransmayr2024_ltbr_igtr. All data needed to evaluate the conclusions in the paper are present in the paper or the Supplementary Materials. Tabulated underlying data for all figures can be found in data file S1.

Submitted 4 June 2024
Accepted 22 October 2024
Published 22 November 2024
10.1126/sciimmunol.adq8796